

Moving forward

A low-cost 3D printed transtibial prosthetic socket for Sierra Leone

J. van der Bie

Technical Medicine | Imaging & Intervention | TU Delft | Radboud University Medical Center | 3D Sierra Leone | Sep 2020 – May 2021 |

Moving forward
*A low-cost 3D printed transtibial prosthetic
socket for Sierra Leone*

By

J. van der Bie

Thesis in partial fulfilment of the requirements for the joint degree of Master of
Science in

Technical Medicine

University Leiden ; Delft University of Technology ; Erasmus University Rotterdam

General information

Student	J. van der Bie (Judith)
Student number	4375149
Master program	Technical Medicine
Track	Imaging & Intervention
Project duration	September 2020 – May 2021

Supervisors

Medical supervisor	Dr. L. Brouwers
Technical supervisor	Dr. Ir. G. Smit
Technical supervisor	Dr. Ir. L. Verhamme
Daily supervisor	M. van der Stelt MSc.

An electronic version of this thesis is available at <http://repository.tudelft.nl/>.

Judith van der Bie

Moving forward: A low-cost 3D printed transtibial prosthetic socket for Sierra Leone

Master's Thesis | may 12, 2020 | Available online at <http://repository.tudelft.nl>

Delft University of Technology | Leiden University | Erasmus University Rotterdam

Technical Medicine

Faculty of Mechanical, Maritime and Materials Engineering (3mE)

Mekelweg 2

2628 CD Delft

The Netherland

Assessment committee

Chairman

Prof.dr.ir. J. (Jaap) Harlaar

Professor of Clinical Biomechanics
Director of Studies for Technical Medicine
Department of BioMechanical Engineering
Delft University of Technology

Medical supervisor

Prof. dr. G.M. (Gerard) Ribbers

Head of Department of rehabilitation
Erasmus MC

Technical supervisor

Dr.ir. G. (Gerwin) Smit

Assistant Professor
Department of BioMechanical Engineering
Delft University of Technology

Daily supervision

M. (Merel) van der Stelt MSc.

PhD candidate 3D Prosthetics
3D lab
Radboud University Medical Center

Preface

Ongeveer een jaar geleden stuiten ik op het 3D Sierra Leone project via een studiegenootje. Met mijn reislustige achtergrond hoefde ik geen moment te twijfelen en dacht direct dit is een project dat op mijn buik geschreven staat. Één mailtje verder en ik had Lars al aan de lijn. Hoe hij sprak over dit project gaf mij direct de motivatie om hier mijn bijdrage aan te leveren.

Als klinische technoloog vind ik het belangrijk om innovatief en creatief te werk te gaan. Iets waar ik mij volledig in kon vinden in dit project. Roeien met de riemen die je hebt want niet alles wat hier in Nederland mogelijk is, is ook vanzelfsprekend in Sierra Leone. Daarom vond ik het ook erg interessant om met verschillende disciplines aan dit project te mogen werken. Hierbij zie je de andere denkwijzen van verschillende disciplines gelijk naar voren komen en waar je als klinisch technoloog echt een verschil kan maken.

Ik zei tegen Merel het belangrijkste vind ik dat ik met trots terug kan kijken op de laatste loodjes van mijn opleiding tot klinisch technoloog en echt een bijdrage kan leveren op het med-tech vlak. In mijn ogen heb ik dit volbracht. Ik heb ontzettend veel geleerd dit jaar niet alleen op het gebied van 3D prothesiologie maar ook hoe ik wil zijn en ontwikkelen als Klinisch Technoloog.

Gerwin en Luc bedankt voor het uitbreiden van mijn kennis op werktuigbouwkundig vlak. Merel bedankt voor jouw kritische begeleiding. Ook in deze rare tijd wist jij mij toch te blijven motiveren en er voor te zorgen dat ik mijn ogen op het grote doel hield, dit was soms niet makkelijk. Maar uiteindelijk verricht je dit werk voor mensen die anders nooit hulp zouden krijgen en dat maakt dit project zo oprecht en mooi.

Helaas door omstandigheden heb ik de impact van het project nog niet in het echt kunnen aanschouwen. Maar ik hoop in de nabije toekomst nog af te kunnen reizen naar Sierra Leone om daar mee te maken welk verschil dit project maakt voor de patiënten daar. Het doel is aan het einde van dit jaar met behulp van mijn onderzoek, een nieuw duurzamer design ontwikkelt te hebben. Ik ben erg benieuwd hoe dit eruit gaat zien en om dit vervolgens in de praktijk te kunnen brengen. Dat is ten slotte het doel, het verschil maken door techniek en medische kennis te laten versmelten voor een duurzamere oplossing voor mensen die het nodig hebben. En ik ben trots op dat ik hier mijn steentje aan heb kunnen bijdragen.

*J. van der Bie
Delft, April 2021*



Table of content

List of abbreviations	x
General introduction	11
Goals and objectives	13
1.2.1 Research question	13
1.2.2 Sub questions	13
1.2.3 Structure of this report	13
2. Biomechanics of an FDM printed tough PLA transtibial socket	15
Abstract.....	15
2.1 Introduction	15
2.2 Socket biomechanics.....	17
2.3 Finite element analysis of the current design	18
2.4 Condyle caps and patella region	21
2.5 Socket adapter interface	24
2.6 Pilot	26
2.7 Discussion.....	26
2.7 Conclusion.....	27
93. Determination of pull-out strength and pull-out torque of tough PLA 3D printed object	29
Abstract.....	29
3.1 Introduction	29
3.2 Method	30
3.3 Results.....	31
3.4 Discussion.....	33
3.6 Conclusion.....	35
4. Influence of thickness, infill pattern and density on the flexural behavior of FDM printed tough PLA	37
Abstract.....	37
4.1 Introduction	37

4.2 Method	38
4.3 Results.....	41
4.4 Discussion	45
4.6 Conclusion.....	47
5. General discussion	49
5.2 Sub questions.....	49
5.3 Future recommendations	50
5.4 Final conclusion.....	52
References.....	53
Appendix A: First iteration design	A
Appendix B: Partial wall thickness.....	B
Appendix C: Results of bending tests.....	E

List of abbreviations

AM	Additive manufacturing
CAD	Computer-aided-design
CAM	Computer-aided-manufacturing
FFF	Fused filament fabrication
SLS	Selective laser sintering
FDM	Fused deposition modelling
PLA	Polylactic acid
ISO	International standard of
FEA	Finite element analysis
GRF	Ground reaction force
PT	Patella tendon
PD	Popliteal depression
LT	Lateral tibia
MT	Medial tibia
ASTM	American Society for Testing and Materials
SD	Standard deviation
3PBT	Three point bending test
ABS	Acrylonitrile butadiene styrene
CS	Cubic subdivision

1.1 General introduction

1.1.1 Problem definition

According to the World Health Organization 40 million amputees are living in developing countries¹. An amputation has a great impact on the quality of life of a patient. In general, patients have limited mobility, often lack of confidence and consequently are at times excluded from participating in society². Prosthetic rehabilitation could help to overcome these obstacles. However, only 5–15% of the amputees in developing countries have access to a prosthesis. Patients are often not able to afford a prosthesis and facilities are not in immediate vicinity^{3,4}.

In 2018, van der Stelt et al⁵ conducted a feasibility study in the Masanga hospital in Sierra Leone to investigate how to aid patients in developing countries with an amputation. It was determined that there is a great demand for affordable leg prostheses since 68% of all amputations in the Masanga hospital in 2018 were lower limb amputations⁵. The average income of a Sierra Leonean is roughly \$490 USD per capita per year, which makes it almost impossible to afford a prosthesis which costs approximately \$100 – 200 USD⁶. To be able to aid these patients, research was conducted on how to produce a low-cost transtibial prosthesis.

1.1.2 transtibial prosthetic

A transtibial prosthesis typically consists of the socket, pylon and a foot component (see figure 1-1). The socket is the most important part considering it is designed to fit the unique shape of the residual limb of the patient⁷. The fitting of the socket is crucial to prevent complications such as discomfort, irritation or damage to the skin of the residual limb. Moreover, if shear and friction become excessive, they may cause pain, dermatitis, hyperhidrosis, blisters, unpleasant odour, infection and bacterial invasion or unwanted wear and tear of the socket^{8,9}. To prevent this, pressure sensitive spots like bony protuberances and tendons are relieved from pressure by removing material of the socket on these sides. On the other hand, to guarantee a secure linkage between the socket and residual limb, material is added in pressure tolerant areas to ensure a tight fit⁹ (see figure 1-2).

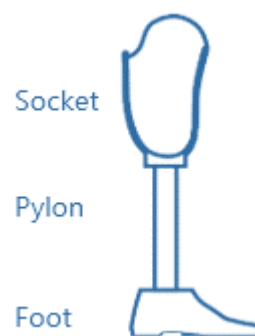


Figure 1-1: Transtibial prosthetic components

The current process of making a prosthetic socket is mainly manual. First, a plaster wrap cast is taken of the residual limb of which a positive mold is created with Paris plaster¹⁰. The positive mold is then

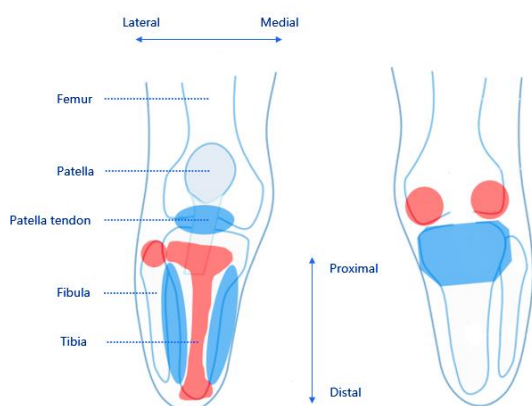


Figure 1-2: Representation of load-bearing sides: lateral and medial of the tibia, patella tendon and popliteal depression (blue) and non-loadbearing sides: tibia, fibula head and tibia condyles (Red).

adjusted by adding and removing material to meet the requirements of the load and non-load bearing sides^{11,12,13}. This process is done by hand and therefore is the socket shape highly depended on the skills and experience of the prosthetists.

To finish the socket, a thermoplastic is directly pulled over the modified positive mold. By this means, both the wrap cast and the positive mold are dissolved during the process, and no record remains of the patient's residual limb geometry. Therefore, if a new socket is required, the entire process often has to be repeated and the second socket will not be identical to the first one¹⁴. Overall, the current process of making a prosthetic socket is time consuming and labor extensive¹⁵.

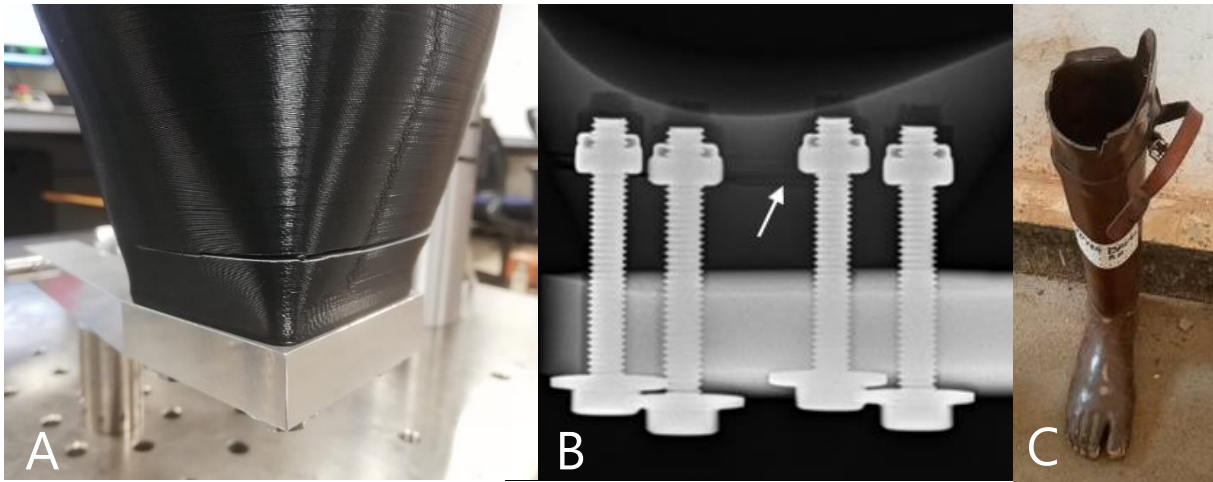


Figure 1-3: Type of failure of the socket. **A:** Crack that occur during dynamic tests after 2.27 million steps. **B:** X-ray image of the crack at the level of the nuts. **C:** Failing of a condyle cap

1.1.3 Additive manufacturing

Additive manufacturing (AM) is the development of 3D objects through a computer-aided design (CAD) or computer aided manufacturing (CAM) by layering material, better known as 3D printing. AM is not restricted by either geometrical complexity or production volume, which makes it a perfect method for unique and accurate design, prototyping and production¹⁶. AM is an emerging technique and with the rapid development it continues to grow and becomes more advanced^{17,18}. It has become easily accessible and relatively inexpensive¹⁶, creating countless opportunities and possibilities in various industries including prosthetic development.

Fused filament fabrication (FFF), better known under the trademark Fused Deposition Modeling (FDM) is one of those 3D printing techniques. FDM creates 3D objects by heating a material filament, often thermoplastic, and depositing it layer by layer on a building platform⁷. Due to the high availability of materials, FDM has a high flexibility. In addition, it is the most cost-effective way of printing due to low part costs and scaling up is easy¹⁹. The strength of the design is however highly dependent on the adhesion between layers and the amount and size of voids present in the object¹⁹. The adhesion and the presence of voids is controlled by various printing factors, still FDM seems promising when these factors are successfully controlled⁹.

Sockets are frequently more printed by the means of Selective Laser Sintering (SLS). SLS uses a CO₂ laser to fuse a layer of powdered polymer material¹⁴. Often limited support is needed when printing since the material itself is an adequate model support throughout building. Because the powder is melted together a strong connection between layers is accomplished. Nevertheless, SLS uses materials which lack structural properties and are often quite brittle²⁰. In addition, SLS objects can only be printed with a solid internal structure, which is sometimes not favorable. Compared to FDM, SLS is more expensive and less accessible. Moreover, there is little literature available regarding the production of FDM printed transtibial sockets. As a result, van der Stelt et al focused on the creation of a transtibial socket by the means of FDM in order to provide a low-cost prosthetic for developing countries.

1.1.4 Current work

In 2019, an FDM tough polylactic acid (PLA) transtibial socket was created by van der Stelt et al²¹ and tested in accordance with International Standard for Structural Testing of Lower Limb Prostheses (ISO 10328)²². This standard specifies procedures for static and dynamic strength tests on a lower limb prosthesis. To pass the static test the prosthesis must be subjected to specific loads. The tough PLA socket passed the ultimate static test with a force of 4025N. Subsequently, the socket was subjected to

the dynamic test. To pass the dynamic test, 3 million steps are required. These 3 million steps are equal to three years of use. Unfortunately, the socket failed after 2.27 million steps with a maximum compressive force of 1200N, due to a crack at the level of the locknuts by which the socket is connected to the pylon (see figure 1-3A/B).

The ISO10328 offers guidance to test the strength for prosthetic parts. The standard does not specifies a test method for the socket itself. At the moment there are no specific tests for the socket and therefore the ISO standard is the most suitable for the strength evaluation of the socket. By means of, it was decided that the socket was safe enough for use in Sierra Leone. In total, 8 patients received an FDM 3D printed transtibial socket. This allowed long-term outcomes to be revealed. Within one year of use two other weak spots of the design were detected: the condyle caps and patella region which failed in two out of the eight cases (figure 1-3C). According to the patients, these sockets failed during normal daily use. The crack that emerged during the dynamic test of het ISO10328, did not occurred in the long-term outcomes.

In summary, a reliable FDM low-cost 3D-printed transtibial socket was created and tested. However, to be cost-effective, the prosthesis has to be more sustainable. On that grounds, more research has to be conducted to create a more powerful design that passes the dynamic test and guarantee a longer life span, to ascertain a more sustainable socket for aiding amputees in developing countries.

1.2 Goals and objectives

1.2.1 Research question

- What modifications are required to ensure a more sustainable low-cost transtibial prosthetic socket design using Fused Deposition Modelling (FDM) in rural areas?

1.2.2 Sub questions

- What are the fragile parts of the current socket design?
- What are the problems regarding the assembly of the 3D printed transtibial prosthetic?
- What are the possibilities to strengthen the fragile parts?
- Is it possible to use less material in order to reduce the costs further while retaining the strength?

1.2.3 Structure of this report

This report consists of 3 chapters. The first chapter contains an analysis of the initial socket design through the use of finite element analysis. The second chapter shows research regarding new methods of assembly the socket to the adapter. The last chapter will investigate the possibilities to use infill instead of a solid design in order to reduce the costs and risk of failure. As a conclusion, a general discussion was written to combine all findings and provide recommendations for a future design and further research.

The image shows two black, smooth, prosthetic limbs standing upright on a white surface against a white background. The limbs are positioned on the left and right sides of the frame. Overlaid in the center is the text 'Chapter Two' in a large, bold, blue font. The text is split into two lines: 'Chapter' on the top line and 'Two' on the bottom line.

Chapter Two

Biomechanics of an FDM printed tough PLA transtibial socket

Abstract

Background

Amputees in developing countries often do not have the opportunity to proper treatment because prosthetic rehabilitation is usually too expensive and facilities are not in reach. To aid these patients van der Stelt et al created an FDM 3D printed low-cost transtibial socket for amputees in the rural areas of Sierra Leone. Nevertheless, during both objective tests of the ISO10328 and long-outcome measurements problems did occur regarding the strength and sustainability of the socket. Therefore, more research had to be conducted to improve the socket's performance and strength.

Aim

The aim of this chapter was to identify the fragile parts of the current socket design and determine the problems regarding the assembly of the 3D printed transtibial prosthetic.

Main findings

Three weak spots were identified through finite element analysis. The first two were found at the patella region and back corners of the condyle caps. In stance, stress accumulations occurred at these regions of 13.8 MPa and 22.6 MPa respectively. The stresses increased during the gait cycle especially during the heel off and heel strike phase. All stress values however did not cross the yield strength of the material. Which most likely indicated that micro stress fractures have occurred during walking due to the higher stress within this regions compared to the overall stress in the complete socket. This presumably caused the socket to fail in Sierra Leone.

In addition, the locknuts that were used within the initial design caused a tear through the print layer during the dynamic testing with accordance to the ISO10328. High stress accumulations (59.7 MPa) were observed within the pockets of the locknuts and at the corners of the bottom part of the socket. These accumulations together with the repetitive load during the dynamic test, caused the printer layers to be separated. This identified the adhesion between the layers as another weak spot of the initial design.

2.1 Introduction

It is important that prostheses are durable especially for patients in developing countries since they cannot afford a new prosthesis repeatedly. Patients often do not live close to a facility that could provide prosthetics and rehabilitation. Moreover, there are only few specialists that can make a prosthesis as well. Since traveling is generally too expensive or too far, there are very few amputees who possess (well-fitting) prosthesis. In addition, these patients live in different living conditions with higher temperatures and humidity than for example the Netherlands. To aid these patients, a prosthesis is needed that is not only inexpensive but likewise is durable and well-fitted.

As mentioned in the general introduction, unfortunately a tear developed in the patella region through the direction of the print layers in 2 out of the 8 cases. In one case the tear propagated through the print layer all the way to the back of the socket. This resulted in the right condyle cap to break off. Additionally, a crack occurred at the level of the locknuts in the initial design. In this chapter those elements will be analyzed and recommendations are set for testing and further research.

To gain insight why the socket has failed at these particular areas, force analyses on the socket have been executed. First, literature research was conducted to determine what forces are at play in the socket during the gait cycle. These forces are used to create a finite element analysis (FEA) of the socket. FEA is a numerical technique to understand and quantify structural behavior of an object²³⁻²⁵. Through partial differential equations FEA predicts how an object behaves under given conditions. It helps to determine weak spots in a design before production, and therefore is very helpful to evaluate the current socket design²³⁻²⁵.

2.1.1 Stress and strain

The strength of a material is based on the ability to endure loads without excessive deformations or failure of the material. The material properties of an object defines this strength. These properties can be determined with tensile and compression tests, where a test specimen is subjected to a controlled compressive or tensile load until failure. When a load is applied on an object, internal stress arises²⁶.

Stress is defined by the density of the internal force on a given surface²⁷:

$$\sigma = \frac{F}{A} \quad (2-1)$$

Where:

- σ = stress in [MPa]
- F = force in [N]
- A = area in [mm]

An object that endures mechanical stress will deform, the elasticity of the material of which the object is made determines the degree of deformation. If the stress becomes too extensive, the object will fracture. Strain is a measure of deformation representing the displacement relative to a reference length:^{26,28}

$$\varepsilon = \frac{L - L_0}{L_0} \quad (2-2)$$

Where

- ε = strain
- L = final length of the fiber [mm]
- L_0 = initial length [mm]

A stress-strain curve shows the relation between stress as a result of an axial load on a material and the relative strain. Tensile tests are specially designed to obtain the stress-strain curve. By means of this curve material properties such as yield strength, ultimate tensile strength and Young's modulus can be determined. These properties are important to consider when creating any design as they roughly predict if an object could endure certain loads²⁶⁻²⁸.

A stress-strain diagram has a typical distribution and starts with a linear elastic region. In this part the stress is proportional to the deformation according to Hooke's Law. Based on the slope of this linear region the Young's modulus of a material can be calculated. The Young's modulus is a mechanical property of stiffness i.e. the resistance to deformation, which is quantified by the relation between stress and strain. The linear region ends with the proportional limit²⁶⁻²⁸.

After the proportional limit, the curve becomes less steep. In this region the material could still behave elastic but with gain in stress, the deformation increases relatively more. The end of the elastic region is defined by the yield point. After the yield point material will endure plastic deformation. Stress is more or less constant but the deformation keeps increasing. After yielding, the material will enter the strain hardening region. The stress will increase but the curve flattens out until the highest tensile strength is reached. During strain hardening the cross-section decreases evenly over the entire length. If a material is brittle it will break instantly at the highest tensile strength. On the contrary, ductile materials will enter the last phase where the cross-section decreases at one point of the specimen. The phenomenon is called necking and results in a small cross-section but large stresses²⁶⁻²⁸.

2.1.2 Bending

In tensile tests an axial load is applied to the test specimen in the direction of the longitudinal axis. But a material can additionally endure bending stress and strain when the load is perpendicular to the longitudinal axis of the specimen. Bending of a material leads to compression of the upper edge of the specimen while the bottom endures the highest tensile stress. A neutral axis runs through the center of the material. No deformations and stress occur at the neutral axis^{26,29}.

Stress during bending can be calculated by the following formula:

$$\sigma = \frac{M * Y}{I} \quad (2-3)$$

Area moment of inertia (I) determines the resistance to bending due to an applied moment. Y is the distance from the neutral axis and M is the moment about the neutral axis. The maximal tensile or compression stress can be found at the farthest edges (c) from the neutral axis^{26,29}

$$\sigma = \frac{M_{max} * c}{I} \quad (2-4)$$

2.1.3 Fatigue

When an object is subjected to a repetitive load less than the ultimate tensile strength and yield strength, the material of the object is likely to be weakened which will subsequently result in failure. This behavior is defined as fatigue and typically arises in parts of the object where the stress is much higher than the average stress in the entire cross-section. For this reason microscopic tears will develop in this particular part. At the ends of these tears new stresses will arise and this leads to further expansion of the tears. Ultimately, the rapid propagation of tears will lead to fracture of the entire structure. To ensure that an object that is repetitively loaded is strong enough for a specific load, it is necessary to establish a safe limit. This limit is called the fatigue/endurance limit and is displayed in an S-N curve, where stress is plotted with respect to the number of cycles. The point where the curve becomes asymptotic is called the limit of endurance

Stress, strain, bending and fatigue are features of interest when designing an object. It could provide a better understanding to define materials that could be used in specific applications³¹. It could be helpful when analyzing a design against failure as well.

2.2 Socket biomechanics

During the gait cycle a repetitive load is applied to the socket. Figure 2-1 shows a figure of the forces and moments during stance where F_{ox} , F_{oy} , and F_{oz} are force components, and M_{ox} , M_{oy} , and M_{oz} are moments about X, Y, Z axes through the center of mass of the socket. During stance the situation is in equilibrium and the ground reaction forces (GFR) counter balance the downward forces of the weight of the patient

Jia et al³² conducted research about the biomechanics and stress distribution of a transtibial residual limb and prosthetic socket during the entire gait cycle. Kinematic data of the lower limb and socket was collected by means of motion analysis and a force platform. In this study the test subject was a transtibial amputee that weighted 81 kg. Figure 2-2 shows the forces and moments at the critical phases of the gait cycle and the neutral position. In stance an axial load proportional to the weight of the patient ($F_y = m * g$) arises, which was counteracted by a ground reaction force of approximately 800 N.

(Note: the F_y depends on the walking speed of the subject. This study investigated the normal walking speed. However, if the walking speed increases the forces increases proportionally.)

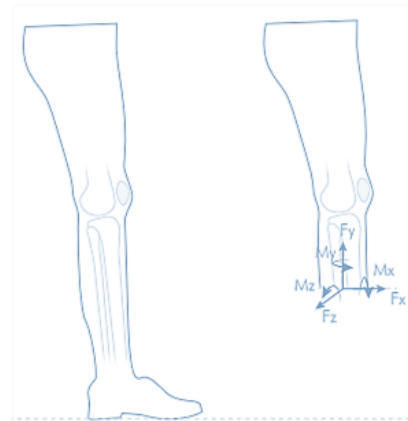


Figure 2-1: Force direction in the prosthetic transtibial socket³⁴

The most critical phases of the gait cycle are during the "heel off" and "heel strike" phase. During these phases a moment (M_z) arises in the socket of 40 Nm and 20 Nm respectively. This moment acts around the center of the interface between the socket and adapter since this part restricts the rotation of the socket itself. The larger moment of the heel off is explainable by the knee joint that pushes the body forward and upward. In heel off the moment creates an extra force in the negative x direction of 100 N, in heel strike a force of 150 N is applied in the positive x direction (see figure 2-1).

Shear stresses between the socket and the residual limb are displayed in figure 2-3. Higher stresses arise on the load bearing sides: the patella tendon (PT), popliteal depression (PD) and lateral and medial of the tibia (LT, MT), as expected. Contact pressures are reported in a range of 20-280 kPa, 180-340 kPa, 90-280 kPa and 60-130 respectively^{32, 35-39}. Likewise, the highest overall von-Mises stress and total deformation within the socket itself occur at the heel strike and heel off^{32,35,36}. The distal end of the socket endures the most von-Mises stress during the entire gait cycle due to the compressive forces between the socket and adapter. According to literature stress of 8 MPa was reported in this interface. The region that endures the second highest stress is observed in the patellar tendon region with peaks of 4 MPa. The posterior, lateral and mid-anterior regions endure less stress³⁵.

2.3 Finite element analysis of the current design

To analyze the stress distribution in the socket FEA's were made in Solidworks (Version 2020-2021)⁴¹. A simplified model of the initial design was sketched with the corresponding dimensions to create a STL file (see figure 2-64) The inside of the socket was divided into multiple areas to apply different shear stresses and forces to individual parts (see figure 2-5).

2.3.1 Boundary conditions

A custom made material was created with the material properties of tough PLA according to the datasheet from its manufacturer Ultimaker⁴² and applied to the design. First the stance phase was simulated by a downward force of 800 N on the bottom of the socket resembling the weight of the patient (yellow area, figure 2-5). Contact pressures were applied on the inside of the socket to simulate the residual limb pressing against the socket. Each area received the corresponding value from figure 2-3. To the orange areas, defined as the non-loadbearing sides, an average pressure of 100 kPa was assigned⁴³. A zero displacement constraint was set at the bottom of the socket to mimic the socket standing flat on a surface. Deformations were set to true. Meshes were calculated as fine as possible to achieve the most accurate stress distribution. The maximal stress value (red) was set to $2.5 * 10^7$ N/m² and the minimal stress value (blue) was set to zero.

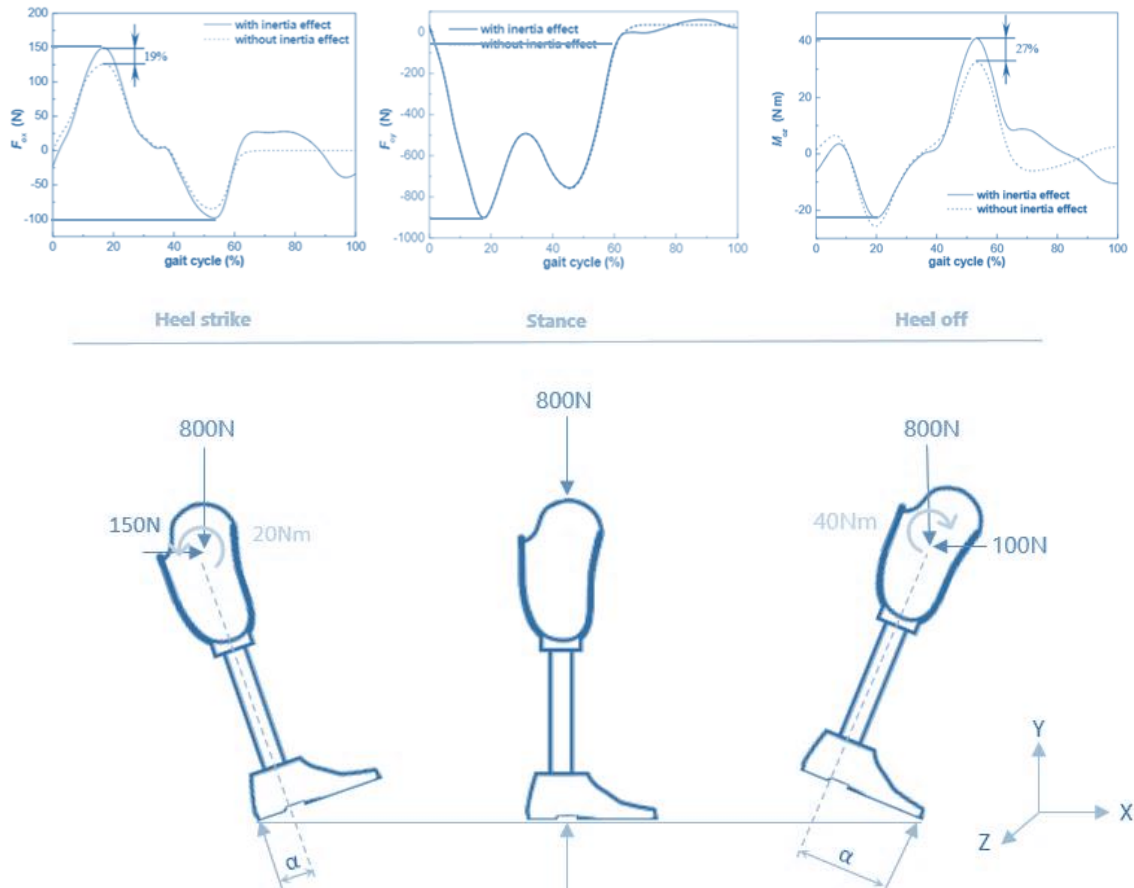


Figure 2-2 Forces and moments on the socket during walking gait. The upper left figure shows the force in F_y direction, the middle figure F_x and the right the moment in M_o . High forces arise at $\approx 20\%$ and $\approx 60\%$ of the gait cycles. At this stage the patient was in heel strike and heel off respectively. The figure below gives an overview of the forces and moment during this phase³²⁻³⁴.

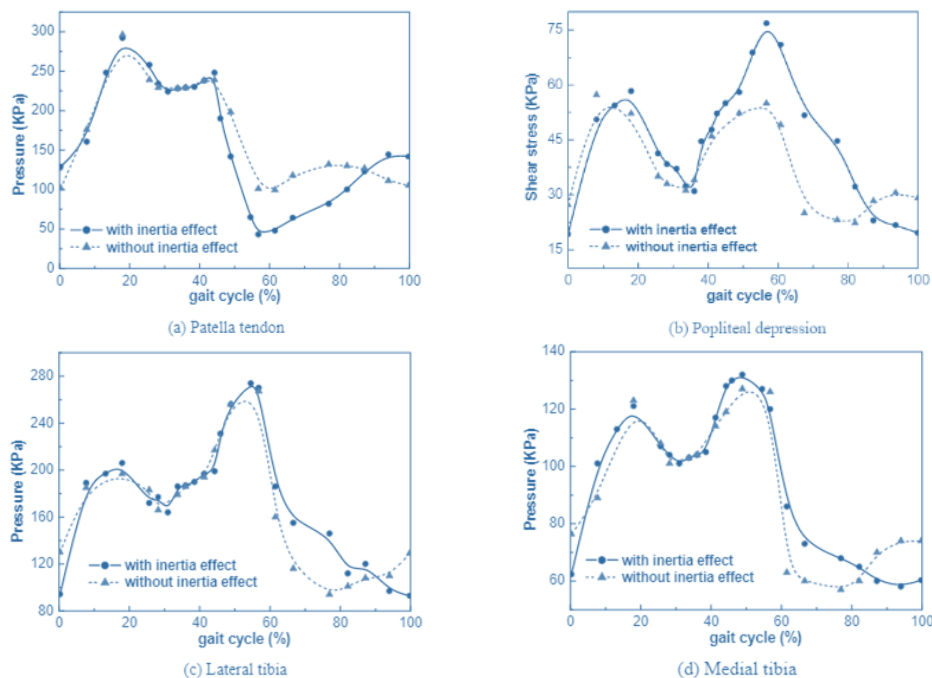


Figure 2-3: Shear stress between the residual limb and the socket of the popliteal depression, patella tendon, lateral and medial side of the tibia. Again during heel strike ($\approx 20\%$) and heel off ($\approx 60\%$) higher pressures arise between the residual limb and the socket. At $\approx 50\%$ the patient is in stance^{32,34}.



Figure 2-4 Initial socket design was measured and those dimensions were converted into simplified STL model. With the values of forces and contact pressure found in literature bounding conditions were set and an FEA of the socket was executed.

To simulate the heel strike and heel off phase, extra forces were applied on the inside of the socket. For heel strike an extra force of 150 N was applied to the front of the socket. The contact pressures were changed to the corresponding values from figure 2-3 at $\approx 20\%$ of the gait cycle. To apply a moment, on the bottom of the socket small new planes were created at the back and front part. These planes restricted the socket from continuous rotation around its own axis. A reference point was added to the most outer edge of the sketch to represent the pivot point. For the heel strike phase the pivot point and a zero constraint was set to the new plane at the back of the bottom of the socket.

For the heel off phase and extra force of 100 N was applied at the back of the socket. The values of shear stress in the socket were changed to the corresponding stress of the phase according to figure 2-3. The pivot point was set to the front of the bottom of the socket to create the moment. Then the FEA was executed.

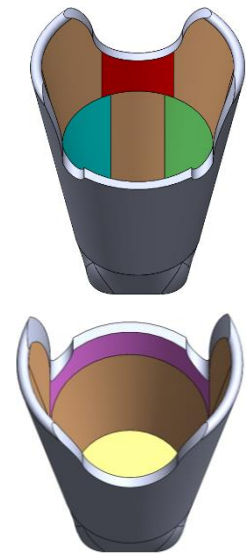


Figure 2-5 Areas within the socket: red patella, cyan medial, green lateral, pink popliteal depression, yellow bottom and orange non-load bearing sides

2.3.2 Results

Stress accumulations in stance were found at the back of condyle caps and at the patella region of 22.6 MPa and 13.6 MPa respectively (see figure 2-6, table 2-1). For heel strike the stress accumulations at the back of the condyle caps (22.6 MPa vs 21.4 MPa) and patella (13,8 MPa vs 15.0 MPa) remained nearly the same. In heel off the stresses increased in the back corners from 22.6 MPa to 29.6 MPa. For the patella region an increase of 2.2 MPa was found in the heel strike phase and 3.2 MPa for the heel off phase (see figure 2-7).

Table 2-1: results of FEA analysis of stress concentrations

	Stress patella [MPa]	Stress condyle caps [MPa]
Stance	13.8	22.6
Heel strike	15.0	21.4
Heel off	17.0	29.6

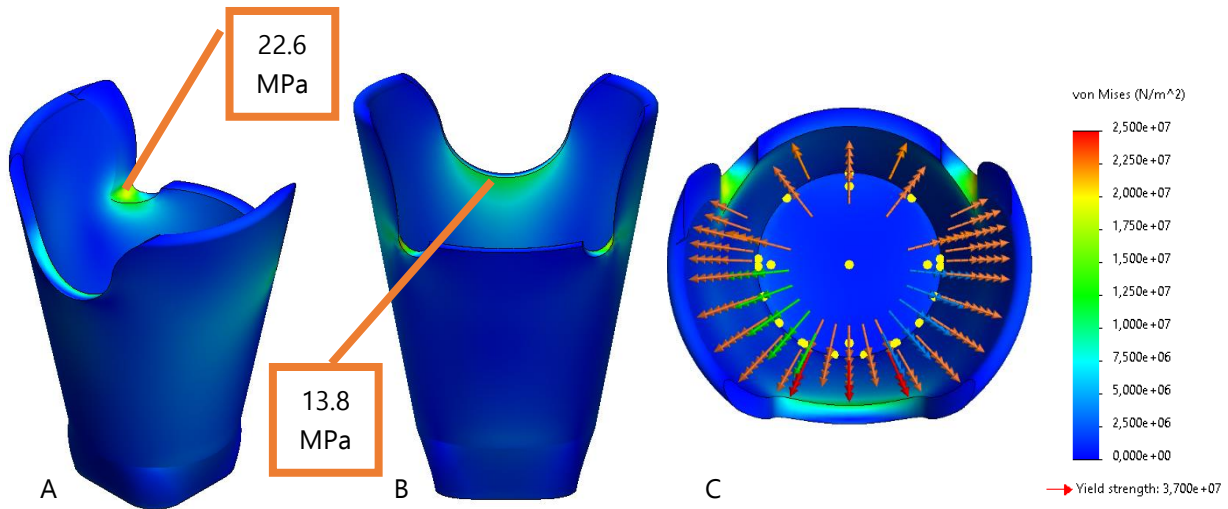


Figure 2-6: The finite analyses of the initial design. **A:** Isometric view of the socket, stress peaks [22.6 MPa) occur at the back part of the condyle caps **B:** Back view of the socket displaying the stress accumulation of the patella region of 13.6 MPa. **C:** Overview of forces: orange 100 kPa, green lateral 180 kPa blue medial 130 kPa, red patella 250 kPa, pink popliteal depression 230 kPa and yellow weight of the patient 800 N.

The values of these stress accumulations remained below the yield strength of tough PLA 37 MPa⁴² and will therefore not lead to immediate fracture of the socket. The repetitive load that occur during walking will presumably fatigue those areas because the stress accumulation are higher than the average stress in the complete socket. This might lead first to microtears that further propagated and eventually lead to the failure that occurred in Sierra Leone. Overall, this analysis has revealed two weak spots of the socket. The next section will discuss a possible approach on how to resolve those weak spots.

2.4 Condyle caps and patella region

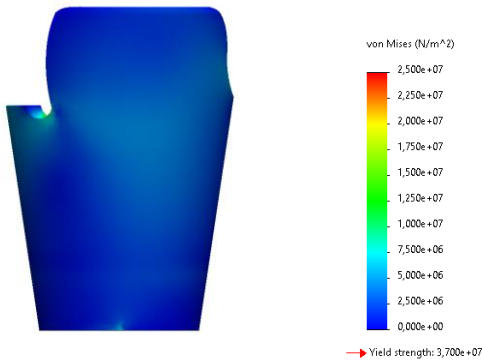
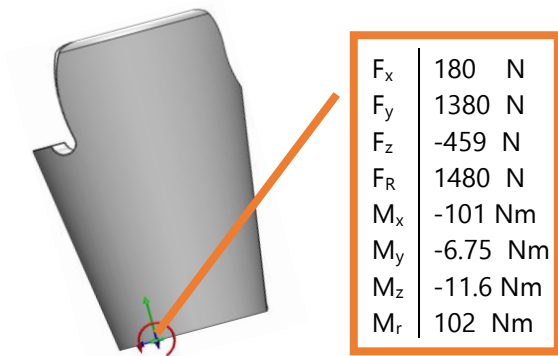
According to the follow-up of the patients from Sierra Leone, a tear developed in the patella region perpendicular to the print direction (see figure 1-3B). The stress accumulations found with the FEA might explain why the prosthesis has failed in this specific area. When walking, the socket must withstand a repetitive load, increasing the internal stress in the patella region and in the back corners of the condyle caps. The increase in internal stress in these small areas in relation to the total area will most likely lead to micro tears, weakening the specific area until eventually the endurance limit is reached. This subsection will discuss methods to decrease the stress accumulations in order to prevent the laceration of the patella region in the future.

2.4.1 Overall wall thickness

The most straightforward feature to lower these stress concentrations is increasing the overall wall thickness. The area moment of inertia determines the resistance to deflection in a particular direction. By increasing this moment a stronger design can be obtained (see equation 2-4). The socket can be approximated as a hollow cylinder. The area moment of inertia can then be calculated by^{25,29}:

$$I = \pi \frac{(r_1^4 - r_2^4)}{4} \quad (2-5)$$

Heel strike



Heel off

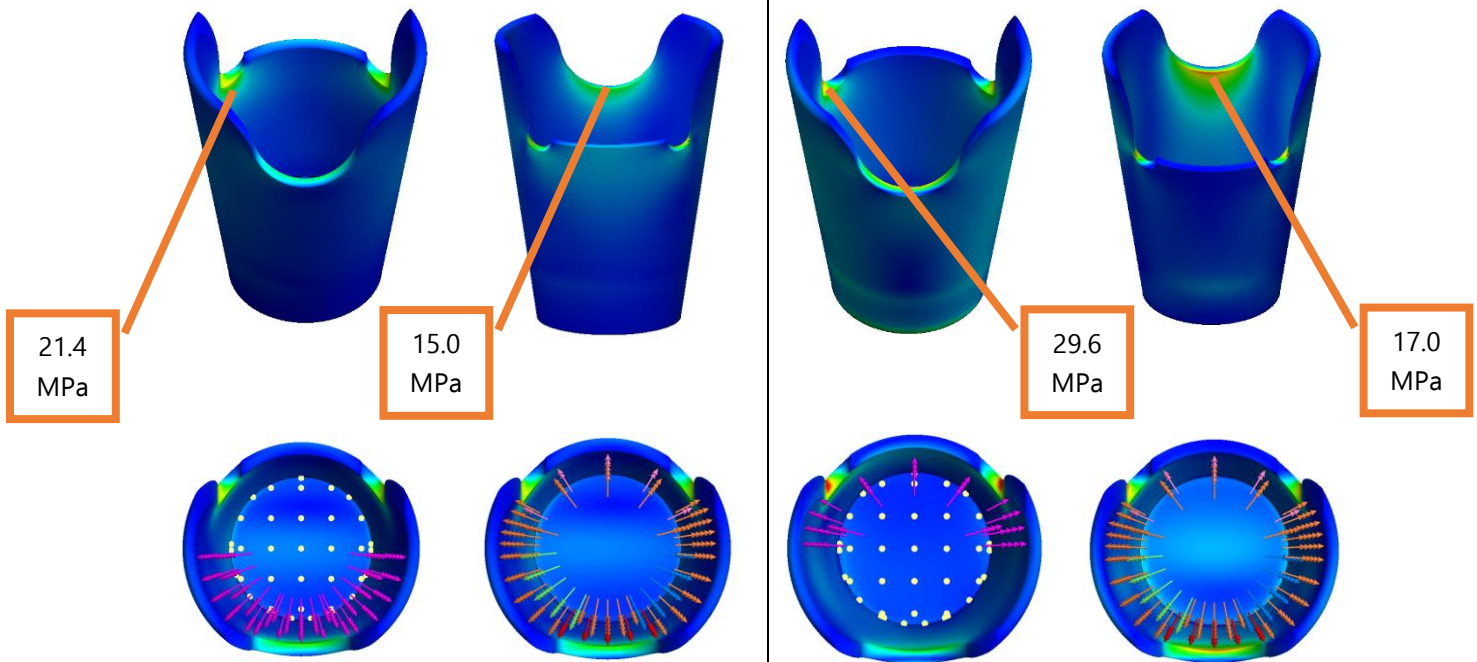
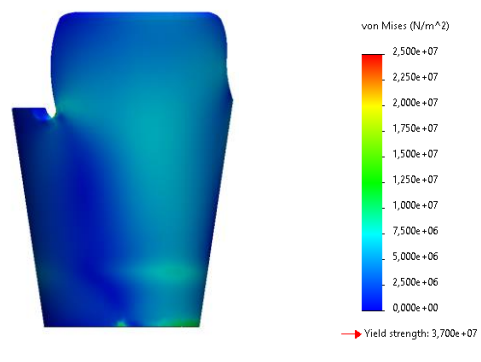
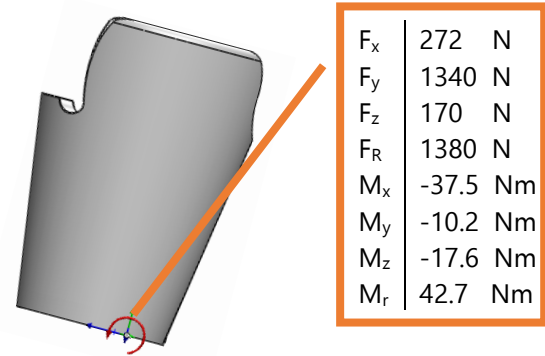


Figure 2-7: Finite elements analyses of the heel strike and heel off phase. The applied forces created a moment in the pivot point of 102 and 42.7 Nm respectively. Higher stresses arose in the patella region in both phases but the stress accumulations in the back corners of the condyle caps only increased in the heel off phase. The last image shows the division of forces: yellow the weight of the patient (800 N) and orange the average pressure of non-loadbearing sides (100 kPa) were kept constant in both simulations. For heel strike the following shear stresses were applied: purple (150 N), Red (275 kPa), popliteal (260 kPa), Lateral (190 kPa), Medial (110 kPa) And for heel off: purple (100 N), Red (75 kPa), popliteal (250 kPa), Lateral (200 kPa), Medial (80 kPa).

Where:

I = area moment of inertia [m^4]

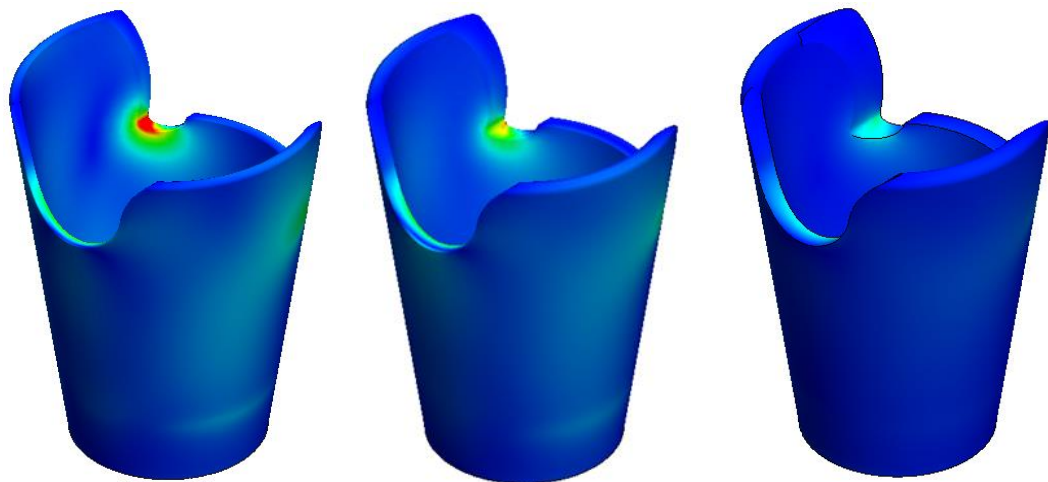
r_1 = the outer radius [mm]

r_2 = the inner radius [mm]

The inner radius (r_2) cannot be changed considering it is conform with the shape of the residual limb of the patient. Increasing r_1 thickness leads to a greater area moment of inertia with a substantial decrease in stress.

To confirm that increasing the overall wall thickness will decrease the magnitude of stress, a short FEA study was executed. The boundary conditions of the stance phase were used and the wall thickness was increased with 2 mm each iteration. The values of the stress accumulations were used as a reference of stress reduction. The color scale was set to from blue (0 MPa) to 25 MPa (red). The goal was to achieve a socket that is as blue as possible, with peak accumulations diffused as much as possible. The results are shown in table 2-2. An increase of 2 mm wall thickness decreases stress with roughly 30%. For example, a socket with wall thickness 4 mm, stress accumulation in the condyle caps of 32.6 MPa occurred respectively to a 22.6 MPa with a wall thickness of 6 mm. Increasing the wall thickness unfortunately does not diffuse stress accumulation over a larger area.

Table 2-2 : FEA for increasing wall thickness. The results show that increasing the wall thickness with 2 mm approximately 1/3 of the stress is reduced in the corners of the condyle caps and the patella region. The increased wall thickness will automatically lead to more material costs and longer printing times.



Wall thickness	4 mm	6 mm	8 mm
Max stress			
Condyle caps	32.6 MPa	22.6 MPa	12.2 MPa
Patella	19.5 MPa	13.8 MPa	7.3 MPa
Weight	315 g	387 g	475 g
Material costs	€20,30*	€24,94	€30,62
Printing time	12 h 47 min	14 h 57 min	17 h 34 min

*Price was based on Tough PLA 750 gram for €48,34 including VAT

Taking into consideration that simply increasing the overall wall thickness will lead to higher costs, longer printing time and no dissolvment of the stress accumulations, the hypothesis arose that it might be enough to only add extra material to the upper part of the socket instead of the whole socket

2.4.2 Partial increasing wall thickness

Ten cate et al³³ performed an extensive FEA in order to determine the area of effectiveness of thickening certain areas in a transtibial 3D printed socket. It was concluded that thickening the lower two third of the socket was not effective to decrease the stresses. The center of the condyle caps and patella should be thickened in order to reduce stress and create a stronger design. If the patella is reinforced, then this must be reinforced over the entire surface up to the condyles. Otherwise, new stress concentrations will appear around the corners of the patella reinforcement³³. In addition, reinforcement of popliteal depression was determined to have relatively little influence³³.

To obtain an optimum between reinforcement and cost, a new FEA study was conducted. A 6 mm thick socket was exposed to 47 FEA analyses, testing several types of reinforcement to determine the best area of effectiveness. Details of this study are found in appendix B-1. The biggest gain (reduction of stress of 38.1%) was obtained when the total surface of the condyle cap was thickened. To use as little extra material as possible but still have substantial reduction, the combination of A1A3 reinforcement was decided to be most suitable which resulted in 36.7% reduction of stress in the back corners of the condyle caps.

Assuming that the tear started in the patella, the patella area must be reinforced as well. Ten cate et al³³ showed that this is only effective when the highest part of the patella is thickened. To verify this another study was conducted (appendix B-2). Although, a small reduction of stress was obtained, it is still encouraged to carry this out in order to create a more sustainable design.

2.5 Socket adapter interface

Not only the condyle caps and patella region were identified as weak spots but the socket adapter interface as well. The prosthetic failed at the socket adapter interface during the dynamic test of the ISO10328²². This standard specifies how to test prosthetic's elements. The socket however is a patient specific element and is not required to comply with this ISO standard. Nevertheless, there are no other standardized methods to test a prosthetic socket which makes this test the most applicable.

The initial socket was exposed to a repetitive load of 50 N to 1200 N at a frequency of 2 Hz. After 2.27 million cycles a deformation of 7.0 mm occurred and the universal test machine stopped automatically. Within this initial FEA analysis no notable stresses occurred at the socket adapter interface. The following section will isolate this part of the socket and will go further into depth.

2.5.1 Static analysis

In the current design a stress fracture occurred in line with the printing direction on the print layer where the top of the pockets of the locknuts are located. The locknuts are placed inside the socket to assembly the socket to the adapter. When the bolts are tightened, the locknuts will apply a force on the print layer which results in a preload on the print layer. An estimation of the preload of the locknut is given by the following formula⁴⁴:

$$F = \frac{T}{\left(\frac{1}{2} * \frac{P + 1.154 * \pi * \mu_{th} * d_2}{\pi - 1.154 * \mu_{th} * \frac{P}{d_2}} + \mu_b * \frac{(D_0 + D_h)}{4} \right)} \quad (2-6)$$

Where:

- T = tightening torque [Nm]
- F = preload [N]
- P = pitch [m]
- D_2 = the mean thread diameter [m]
- D_h = bolt head diameter [m]
- D_h = diameter of the bolt shaft [m]
- U_{th} = friction coefficient in the threads
- U_b = friction coefficient under the torque nut

Currently M6x20mm galvanized DIN 7991 locknuts and M6x20mm screws Galvanised, DIN 7991 are used. The maximal tightening torque was determined with the AOK adjustable window torque wrench (see chapter three). The maximum tightening torque for the initial design was 3 Nm. Friction coefficients are defined by $U_{th} = 0,16$ (table 8-12b) and $U_b = 0.18(13)$ (table 8-12c)⁴⁵. Filling in the values resulted in:

$$F = \frac{3}{\frac{1}{2} * \frac{(0.001 + 1.154 + \pi + 0.16 + 0.00535)}{\pi - 1.154 * 0.16 * \left(\frac{0.001}{0.00535}\right)} + 0.18 * \frac{(0.01344 + 0.0066)}{4}} = 4481N$$

A preload of 4481N was calculated. With this given preload, stress could be calculated within the pockets according to equation 1-1. The area of a hexagonal object is given by:

$$A = \frac{(3\sqrt{3} * s^2)}{2} \quad (2-7)$$

S = edge = 5.92 mm

Together with the formula of stress (1-1):

$$\sigma = \frac{F}{\frac{(3\sqrt{3} * s^2)}{2}}$$

$$\sigma = \frac{4481}{\frac{(3\sqrt{3} * 5.92^2)}{2}} = 49.1 \text{ MPa}$$

This calculated stress is comparable with the ultimate tensile strength of tough PLA of 47.2 MPa determined by van der Stelt et al²¹. This demonstrates a crucial weak spot of the current design. To create a better understanding of the forces in the bottom part of the socket, an FEA of the coupler i.e. the bottom part was made in Solidworks. The coupler was sketched in Solidworks with the corresponding dimensions. The custom-made tough PLA material was applied and a zero displacement constraint was set at the bottom of the coupler. An axial load of 800 N was applied to represent the weight of the patient. The tightening moment of the bolt was simulated with a moment of 3 Nm and a friction coefficient of 0.16. A galvanized steel material was applied to the bolt. High stress concentrations (≈ 60 MPa) appeared inside the pockets of the locknuts, as predicted (see figure 2-8). Stress concentrations arose on the corners of the coupler because there is an irregularity in the geometry that interrupted the flow of stress. The square bottom of the socket in combination with applied forces when tightening the locknuts, makes this region prone to failure.

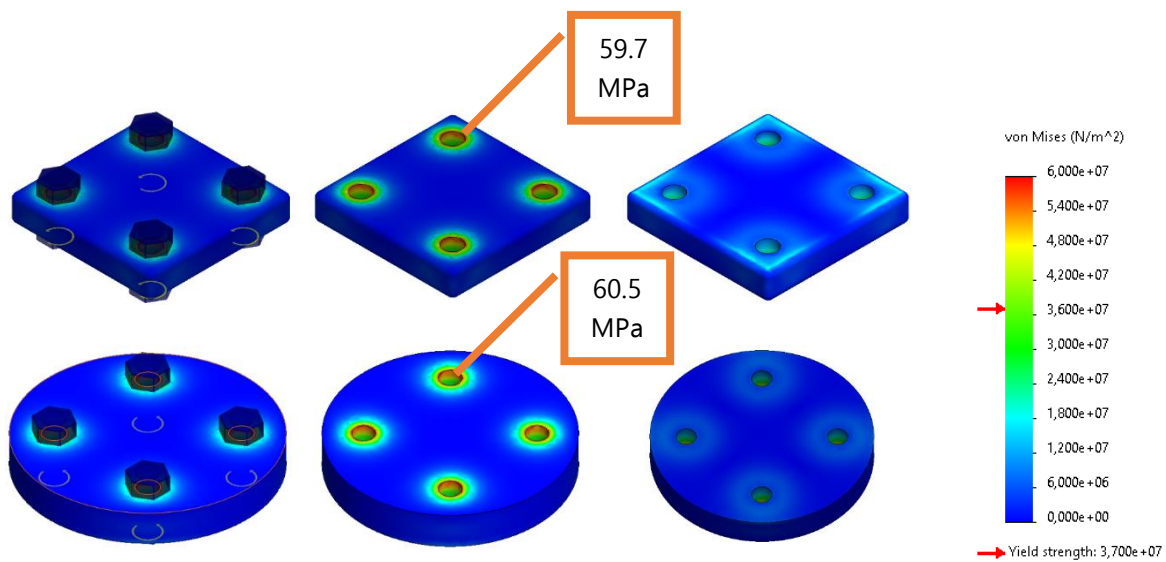


Figure 2-8: FEA of the coupler. The stress concentrations at the corners of the coupler are resolved when a round surface is used. The accumulations on the print layer is still evident and can only be resolved by using another assembly method.

In general, round surfaces are able to continue the flow of stress better and therefore, no stress concentrations should appear. To compare the results to a round surface, the coupler was rounded. All other conditions were kept the same. The concentrations at the level of the locknuts were comparable. At the bottom of the round coupler no stress concentrations occurred, which makes round surfaces more favorable. The high stress concentrations in the cavities remained to exist through the use of the locknuts. To decrease these stress levels, other ways of assembly that divides the forces over various printing layers should be implemented.

2.5.2 Fatigue analysis

Prosthetic sockets frequently fail at the distal region where the pylon is connected to the socket due to the local bending^{11,13,46}. Due to the tensile and compression forces during walking, fatigue will occur. It will start in regions with high stress concentrations (i.e. the locknuts and sharp corners like the back corners of the condyle caps) and expand further until failure. In addition, the higher moments that arise in the interface during heel strike and heel off, will make the bottom part more likely to fracture at the specific area. To the knowledge, no S-N curves of tough PLA are available. More research needs to be conducted to establish the endurance limit of tough PLA in order to make better predictions about fatigue failure of tough PLA.

2.6 Pilot

To aid the patients in Sierra Leone whose prosthesis had failed, a new socket was printed with two adjustments. The coupler part of the socket was made round instead of square. In addition, the overall wall thickness was increased from 4 mm to 6 mm. Other features must be further tested before it can be safely used by the patient. From November 2020 until May 2021, no failure has been reported.

2.7 Discussion

To summarize, this analysis of the socket showed that stress arises at the patella region and back corners of the condyle caps due to the contact pressures and the forces during the gait. The moment that arises in the interface of the socket and adapter, together with higher stress concentrations on the printing layer on which the locknuts are tightened makes this region prone to failure as well. Literature search was conducted to provide methods to overcome these weak spots. A review was written and several options emerged. The easiest manner to increase strength is using materials with higher density or/and increasing the wall thickness of the socket¹⁶. Although, a thicker wall could achieve a better structural integrity⁴⁷, it likewise contributes to a heavier prosthesis and extra costs, which makes it less favourable (see table 2-2). Materials with high elastic modulus and higher tensile strengths could

reduce the weight and wall thickness, while maintaining the strength⁴⁷. Unfortunately, these strategies will not resolve the accumulations, since the geometry of the socket is not changed.

According to literature homogeneous material failed to represent the stiffness and flexibility of skin and muscles⁴⁸. Pressure can be reduced through the use of softer/less material^{12 48}. Generally, when this strategy is applied, the wall thickness of the socket remained the same. Printing two different materials simultaneously can be accomplished by using for instance multi material printing. Only brittle materials however are currently available for this technique which makes it unsuitable for creating a prosthetic socket yet.

Adhesion between layers is very important for 3D printed objects. The adhesion determines the strength. The quality of adhesion is associated with many process-related factors such as: slicing, temperature and printing speed^{16, 33, 35}. Up and until now, the printing profile socket is not researched and was set by a consultant. It would be interesting to research how several printing settings affect the strength of the socket design. It might influence the strength to such an extent that the socket becomes more durable. Further research should be conducted on methods to create better adhesion and their effects on socket strength in order to confirm this hypothesis.

Lastly, another approach is changing the infill density or internal orientation. Regarding infill density and shape, there is a significant relationship between infill and stiffness⁴⁹. It is stated that the infill density and shape contribute substantially to greater rigidity, deformability and longer durability and it is therefore worth investigating further^{16, 49}.

2.7.1 Limitations

This study had some limitations that should be taken into consideration. Within the FEA it was assumed that the material was linearly elastic, homogeneous and isotropic which is not the case in practice, and therefore the 3D printed material behaves differently after a new print. In addition, Solidworks considered the socket as one solid entity. While in reality adhesion between layers of 3D printed objects is crucial for its strength. If Solidworks took this into consideration the design might have been weaker than the solid object that was subjected to the loads within the current analysis.

In addition, the values of shear stress has been derived from multiple articles, the forces during gait only from one article. The article from Jia et al³² performed extensive calculations and measurements of force during the gait and used as the fundament for other articles and their calculations^{33,34}. However, including other values from different articles and forces at different speeds could provide a broader analysis of the stresses within the socket.

No dynamic analyses were performed. To gain more insight in what the effect is of shear stress between the print layers and tensile/compressive repetitive load during the gait, a dynamic analysis could be performed. This first analysis however provided a proper approximation of the stress within the socket and a good insight into where the socket's weak spots are. Broader analysis might lead to more accurate values and a better prediction of endurance of the socket.

2.8 Conclusion

In conclusion, three weak spots were defined on the initial socket design: the patella region, the back corners of the condyle caps and the interface of the socket and adapter. Finite element analysis revealed stress accumulations in the first two weak spots that arose due to the contact pressures and forces during gait. This was uncovered in daily use of the prosthesis in Sierra Leone as well. The interface between the socket and adapter failed during the dynamic test by means of the use of locknuts, sharp corners of the bottom and the adhesion of the layers.



Chapter three

Determination of pull-out strength and pull-out torque of tough PLA 3D printed objects

Abstract

Introduction

The assembly of 3D prints can be simplified by the use of threads. Embedding threads into the 3D print could increase their functionality. Currently in the transtibial socket locknuts are used to assemble the socket to the pylon. The use of locknut considered impractical because to embed them, the printer must be paused. In addition, during the dynamics test according to the ISO10328 a crack occurred at the level of de locknuts identifying the locknuts as a vulnerable point. Therefore, the aim of this study was to determine the most suitable assembly method for tough PLA printed parts.

Method

Three different assemblies were tested: a threaded insert, a brass insert and a locknut. The assemblies were embedded in 3D printed tough PLA cubes. Torque-out strength was determined by the means of an adjustable torque wrench. The pull-out test were executed in the Ametek test Lloyd LR5K universal test machine until failure. Data was analyzed with MATLAB and statistical analysis was performed with a one-way ANOVA test.

Results

The torque-out strength for all three assemblies were comparable. The threaded insert was found substantial weaker (4534.10 N) than the brass and locknut in terms of pull-out strength, The brass insert and locknut completed the pull-out test without failure (4825.83 N vs 4834.37 N). However, air pockets were found within the locknut samples after the pull-out tests, indicating internal damage and a less reliable connection.

Conclusion

The brass insert might be the most suitable option for assembly since they had comparable torque-out and pull-out strengths to the locknuts that are currently used in the initial design. Supplementary, the brass inserts contribute to more benefits. First, the brass insert are easier to embedded into a 3D printed part since the printed does not need to be paused. In addition, they presumably divide the stress accumulations found within the FEA with the use of locknuts over multiple layers instead of one. This might contribute to fulfill the complete dynamic test according to the ISO10328 which gives the opportunity to produce the socket in the Netherlands in the near future as well.

3.1 Introduction

Fused deposited modeling (FDM) is a widely used 3D printing technique for prototyping, production, research and education⁵⁰. This technique creates 3D printed objects by depositing material layer by layer, mainly thermoplastics, on a building platform⁷. After depositing the material binds to the layer below and solidifies to a solid-state end product⁵¹. Due to its short cycle time, its high-dimensional accuracy, its ease of usability, and its potential to be easily integrated with different CAD software.^{14,52,53}. Recent advancements make FDM a promising technique for the fast production of highly accurate products in the future⁵².

In order to increase the functionality of a 3D print, the inclusion of threads, to assemble and disassemble different parts of the final prototype/product, could be beneficial. The simplest way of adding threads is by incorporating them directly into the 3D print. However, this has been found not

to be ergonomic and efficient^{6,7}. Integrating metal threads into the 3D printed material contributes to a stronger design and a more simplified approach to manufacture^{54,55}.

Regular nuts are one of the most straightforward and inexpensive solutions for adding metal threads to a print. The nuts can be embedded in a print by means of pockets in which the nuts can be placed. Nevertheless, it can be difficult to design the perfect fit. In case the pockets are too large, the nuts will be able to rotate slightly. This makes it more complicated to tighten the bolts. When the pockets are too small, the nuts will not fit properly, which might complicate the integration of the nuts into the 3D printed part.

Inserts that are specially designed for adding threads to a 3D print have recently been made available. By heating an insert and pressing it into the 3D printed part, a thread is added to the object. As the insert is heated, its surrounding material melts together and binds to the insert. This heating aspect might cause increased adhesion in the layers around the insert, and potentially making these layers substantially stronger. However, so far, little research has been conducted with regard to this subject.

The many inserts currently available, can be roughly divided into two main groups: smooth and threaded. To study the behaviour of these assemblies in a 3D printed object, two properties were tested: the torque-out strength and the pull-out strength. The torque-out strength determines at which tightening torque the 3D print or assembly starts to fracture. The torque-out strength is directly proportional to the pretension force in a bolt. Higher torque-out forces makes an assembly more reliable since it is harder to overtighten the bolt. Moreover, it also makes the part more resilient to damage. The pull-out strength defines how much axial load an assembly can endure until it fails. This is important, as it evaluates to which assembly more tightening force can be applied and which assembly can bear more load. The aim of this study was to determine the torque-out and pull-out strength of three different assembly mechanism, in order to be able to establish the most suitable connection for tough PLA printed parts.

3.2 Method

3.2.1 Study design

Three different connections were tested: a locknut (M6 Gamma), a threaded insert (M6, Karwei) and a brass insert (M6, Ruthex) (see figure 3-1). For every connection six tough PLA cubes of 30x30x30mm with a screw hole were designed in Soliworks³⁸ and printed by a Ultimaker S5. All print settings are summarized up in table 3-1. For the locknut connection a hexagonal pocket was designed with a screw hole with a diameter of 7 mm representing the initial assembly method of the transtibial socket. After three hours of printing, the printer was paused, after which the locknuts were heated and placed in the



Figure 3-1: Three types of connections including price a piece: locknut (€0,22), threaded insert (€0,44), brass insert (€0.33)

Table 3-1: print settings for the test samples

Material	Tough PLA
Printer	Ultimaker S5
Print temperature	225
Print speed	45 mm/sec
Nozzle size	0.8 AA
Bed temperature	60
Layer thickness	0.2 mm
Flowrate	1
Bottom layers	3
Top layers	3
Infill	Concentric
Infill percentage	100 %

insert the outer a diameter of 12 mm was measured. Subsequently, a smaller shaft diameter of 11.6 mm was printed.

3.2.2 Torque-out strength

The cube was placed in a vise. The bolt was tightened with an AOK adjustable torque wrench TWW until the print, connection or bolt failed. The torque wrench was able to generate a torque from 3 Nm to 15 Nm in intervals of 2 Nm.

3.2.3 Pull-out strength

The pull-out strength tests were performed in Ametek test Lloyd LR5K universal test machine. The test protocol of the ASMT C900-19 was adapted. This standard describes a pull-out test for screws in concrete. Fixtures were designed and made to executed these test. All bolts were tightened with 3 Nm with the aforementioned torque wrench. Then the cubes with the tightened bolt were placed into the fixtures (see figure 3-2). To measure the pull-out strength a gradual axial force with a constant rate of 3 mm/min displacement was applied. A load cell of 5000 N was used. All tests were executed until failure or a maximum load of 5000 N was reached.



Figure 3-2: Test-setup for the pull-out tests

3.2.4 Data analysis

Data was visualized in MATLAB R2017B⁵⁶. Statistical analysis was performed using the SPSS version 25 software (SPSS Inc., Chicago, IL, USA)⁵⁷. Descriptive data were expressed in mean \pm standard deviation, (SD), standard error and confidence interval of 95%. For statistical analysis an one-way ANOVA test was executed together with a test of homogeneity of variance and Games-Howell post hoc test. A p-value of <0.05 was considered as statistical significant.

3.3 Results

3.3.1 Torque-out

All torque-out forces are shown in figure 3-3. The locknut connection failed at the lowest torque of 3 Nm. When the bolt was tightened, it could easily be further overtightened with the torque wrench. Causing the locknuts to rotate around Their own axis and the bolt to be screwed into the 3D printed material. In the end, bolt came out of the bottom of the cube with the use of minimal force (see figure 3-4A). Remarkabilities, in the direction of the printing layers could be observed on the outside surface area of the cube. To investigated this x-rays images were made of the 3D printed cubes. However, no internal damage was found.

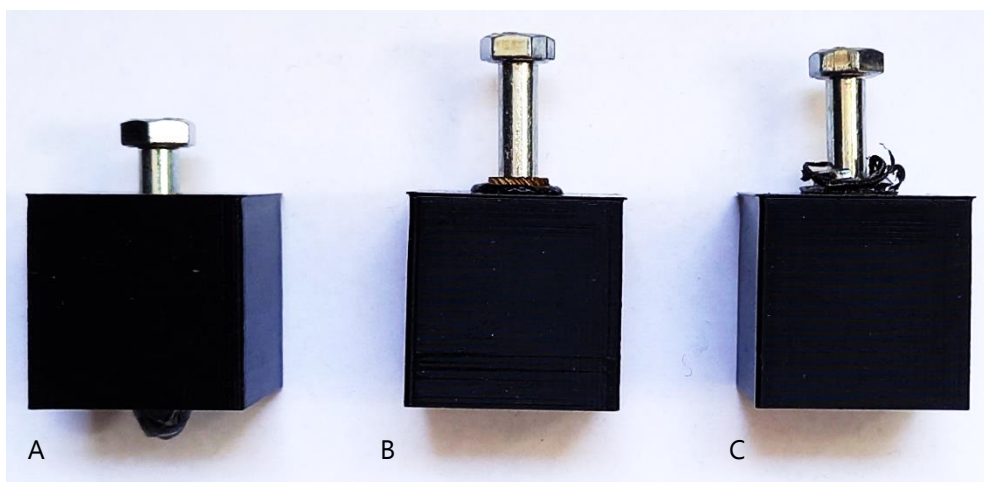


Figure 3-4: Results torque-out tests: A: locknut connection, B: brass insert with light upwards migration. C: threaded insert separated from the material due to the torque.

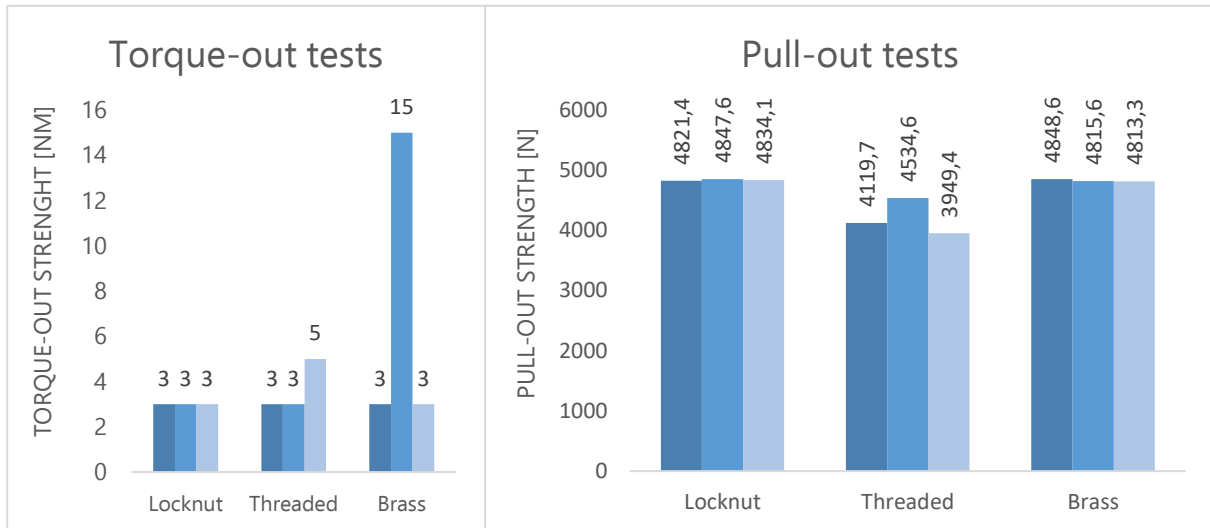


Figure 3-3: Results of torque-out tests for each test sample separately. One test sample (#2) of the brass insert complete the full test.

Figure 3-5: Results of pull-out tests for each test sample separately. The threaded samples showed lower pull-out forces for failure than the locknut and brass inserts samples.

An average moment of 3.67 Nm caused the threaded insert to detach from the print. After failing, the insert rotated around its own axis in the shaft. Comparable to the threaded inserts, two brass inserts failed at 3 Nm and were unscrewed from the 3D print as well (see figure 3-4B/C). Moreover, the loosening of the insert also caused the insert to migrate upwards. One of the brass inserts reached to the highest measurable torque of 15 Nm. The insert stayed perfectly in place but the bolt was screwed into the print and came out of the bottom of the cube similar to the locknut connection.

3.3.2 Pull-out strength

Both the locknut and the brass insert completed the full pull-out tests without failure with an average pull-out force of 4834.37 N and 4825.83 N respectively. The threaded insert failed earlier on average at 4201.10 N (see table 3-3). Two of out of the three cases the threaded insert was completely pulled out of the 3D printed cube (see figure 3-5). All testcases are displayed in figure 3-6.

Table 3-2 descriptive data torque-out tests

	Mean torque [Nm]	Std. Error	95% Confidence interval	
			Lower Bound	Upper Bound
Locknut	3.00 ± 0	0,00	3.00	3.00
Threaded insert	3.67 ± 0.67	0.67	0.80	6.54
Brass insert	7.00 ± 6.93	4.00	-10.21	24.21

Table 3-3: descriptive data pull-out tests

	Mean pullout [N]	Std. Error	95% Confidence interval	
			Lower Bound	Upper Bound
Locknut	4834.37 ± 13.10	7.56	4801.82	4866.91
Threaded insert	4201.10 ± 301.17	173.88	3452.96	4949.24
Brass insert	4825.83 ± 19.75	11.40	4776.77	4874.90

3.4 Discussion

This study tested three possible connections for the assembly of 3D printed tough PLA objects. The torque-out test showed minimal difference between the three types of connections. The locknut connection failed at the lowest measurable torque. The bolt could be easily screwed inside the 3D printed material. The threaded insert failed at 3/5 Nm because the insert was separated from the material. These results are coherent with similar torque-out tests with PLA^{55,56}. The most interesting finding was that the brass insert did not fail. The other two samples of the brass insert were detached from the 3D printed cubes comparable to the threaded insert. The third sample stayed perfectly in place at 15 Nm, but the bolt was screwed into the 3D part, actively demonstrating that the material was the weak factor and not the insert itself.

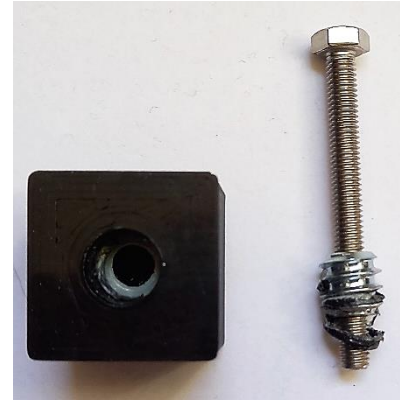


Figure 3-6: Threaded sample pulled out of the cube during the pull-out tests

The pull-out tests showed that the brass inserts and locknuts had comparable results (4847 N vs 4848 N $P = 0,817$). X-ray images showed that within the locknut connection, failure inside of the cube had occurred. In all cases the locknut was migrated upwards, creating a bigger pocket in which the locknut is located. This allowed the locknut to move more freely, making the connection no longer completely reliable (see figure 3-7).

The threaded insert failed with an average force of 4534.6 N but not significantly earlier than the other two connections (vs locknut $p = 0.121$, vs brass insert $p = 0.123$). Considering that the pull-out strength is related to geometric factors that increases the contact surface area between the connection and the surrounding material, overall length of the connection and number of threads, it was not expected that the threaded insert would fail prematurely due to the large threads of the insert i.e. a large surface area on the outside of the insert^{58,59}.

Shear strength describes how two surfaces slide over each other. A higher shear strength often indicates that a higher load is needed to separate two parts. To some extent, shear stress determines the strength between the connection and material. According to the Von-mises theorem, a failure criterium, the ultimate shear strength for ductile materials could be approached by the ultimate tensile strength divide by $\sqrt{3}$. The ultimate tensile strength of tough PLA is roughly 47.2 MPa²¹. By multiplying this value with the shear area of the connection, the theoretical failure load can be calculated:

$$U_{ss} = \frac{UTS}{\sqrt{3}} \quad (3-1)$$

$$U_{ss} = \frac{47.2}{\sqrt{3}} = 27.25 \text{ Mpa}$$

$$F_{ultimate} \approx U_{ss} * A_{shear} \quad (3-2)$$

Where:

$$A_{locknut} \approx 419.72 \text{ mm}^2$$

$$A_{threaded} \approx 648.67 \text{ mm}^2$$

$$A_{brass} \approx 910.53 \text{ mm}^2$$

Gives:

$$F_{\text{ultimate}} \approx 27.25 * 419.72 = 11437.67 \text{ N}$$

$$F_{\text{ultimate}} \approx 27.25 * 648.67 = 17677.03 \text{ N}$$

$$F_{\text{ultimate}} \approx 27.25 * 910.53 = 24812.85 \text{ N}$$

This theoretical values showed that due to a higher area the threaded insert should be stronger than the brass insert. During the tests however, this was not the case. This can be explained by that 3D printed materials are anisotropic and inhomogeneous which makes it difficult to predict their material behavior. Additionally, the assembly is highly dependent on the specific placement and orientation of the insert in the screw hole. Since no recommendations with regard to the diameter of the threaded insert could be found in literature, knowledge of experts was utilised to come to an outer diameter that has been reduced by 0.4 mm. To confirm this a tough PLA cube was printed with multiple diameters. The threaded insert was heated and pressed into the prior designed hole with a soldering iron. A diameter of 12 mm was too big, as the insert could be easily pulled out by hand. The diameter of 11.2 mm was too small and allowed the liquefied tough PLA to leak inside of the insert. This led to obstruction of the insert so that a bolt could not fit anymore. For this reason is assumed that a diameter of 11.6 mm was a proper fit for this type of insert.

Moreover, the process of heating the insert might influence the strength of the connection. Heating the insert increases the adhesion of the layers around the insert, inherently strengthening the connection. During the heating process all inserts were heated for 20 seconds with a gas burner. The actual temperature might influenced the strength of the connection. The impact of the temperature on the connection was beyond the scope of this study.

For safety reasons it was decided to pull the cubes against the fixture instead of putting the cubes inside a clamp. Although a gap within the fixture that has minimal surface overlap with the test sample was designed, this overlap still might have affected the results of the locknut connection. The locknut is broader than the screw hole of the bolt, as a result the locknut rested on a print layer and all material above the print layer. During the pull-out test the locknut is ideally pulled out perpendicular, this type of removal has characteristics of an 'ideal failure" (see figure 3-8). Ideal failure is however not applicable due to the heterogeneity of the material. This make the load of the locknut diffuse over a bigger area which is often results in a bigger angle defined as "real" failure in figure 3-6. Because the cube is pressed against the fixture, compression on the top layer will occur. This compression might influence the real strength of the locknut, resulting in a stronger connection.

In view of the 3D printed transtibial socket, this study has shown that brass inserts are comparable in terms of torque-out and pull-out strength to the current used locknuts. The brass insert have different

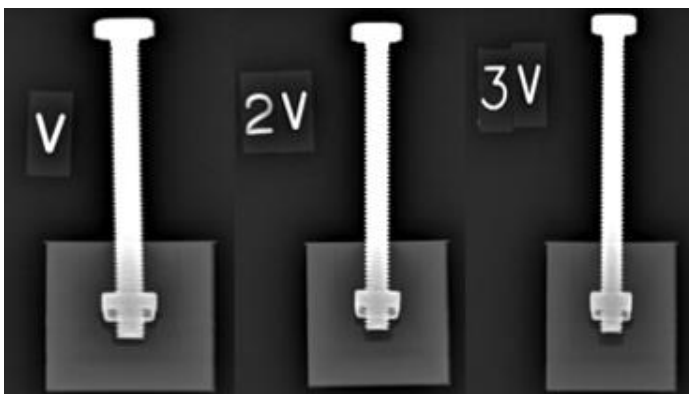


Figure 3-7: x-rays images of the locknut sample were immigration of the locknut is seen by the black spots underneath the bolt-nut connection

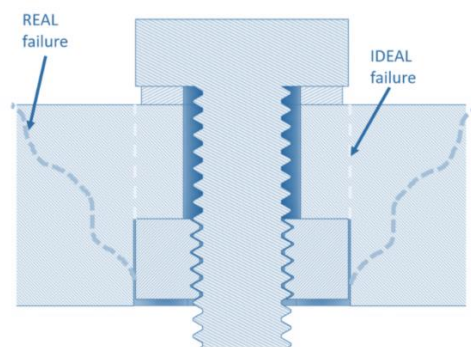


Figure 3-8: Ideal failure of a locknut in material relative to actual failure

orientations of notches on the bottom and top part. The notches are diagonal and opposing pattern relative to each other. This might supplementary prevents the insert from rotating and moving during the tests. Heating the insert presumably improved the adhesion of the layers around the insert, making the insert more resistant to failure. In addition, the insert divides the shear forces over multiple printing layers since it is not resting on a print layer like the locknut. Moreover, the use of inserts might aid to complete the full dynamic test of the ISO10328 because of this division.

The use of inserts is an easy method to integrate threads into a design and is relative inexpensive comparable to the locknuts (€0,22 vs €0,33). In this study a drill pressed was used to embed the inserts but in Sierra Leone this can be easily done with a soldering iron. In addition, through the use of inserts the printing process is simplified because the printer does not have to be set on pause and the product can be assembled directly after the socket is finished printing.

3.5.1 Limitations

The torque wrench in this study had intervals of 2 Nm. The size of the intervals may have been too large as most samples failed at 3 Nm, which was the lowest measurable torque. Unfortunately, there was no torque wrench available with lower measurable tightening torques and smaller intervals.

Although positioning the inserts into the screw hole of the cube was standardized as much as possible, variations were nevertheless experienced. It was difficult to determine the depth of the insert and therefore some inserts were pushed deeper in the cube than others. In addition, the speed at which the insert was pushed into the material affected how the material formed around the insert. This is a plausible explanation for the differences in the torque-out tests of the brass inserts. A more suitable fit with respect to the other samples, could be a potential explanation for the insert that remained in place during the experiment.

In addition, no standard is described how to perform pull-out tests of 3D objects. ASTM C-900 was used as guidance and literature was conducted about similar tests to create an accurate test protocol. To compared the results to other studies more standardized test must be created for testing 3D printed materials.

The fixtures might have influence the exact strength of the connection especially that of the locknut. To make this effect minimal as possible, the overlap between the surface of the fixture and cubes was kept minimal. If the fixtures influenced the strength of the locknut connection, this only made it stronger. The exact influence of the fixture might be less relevant as the brass insert showed similar results already and the strength of the inserts was not affected by the fixtures. By this time defining that the brass insert was a good alternative to the locknut

3.6 Conclusion

This study demonstrated that brass inserts might be the most favorable option for assembly of 3D printed tough PLA objects. Threaded inserts do not contribute to pull-out or torque-out strength as is the case with brass inserts and locknuts. Embedding locknuts is a suitable alternative and easily accessible but requires a more complex design. The brass inserts were easy to integrate into the design and had similar outcomes strengths as the locknuts. The prediction of material behavior of 3D printed objects however can be challenging. Especially, when the heating process and speed of the placement of the insert might affected the strength of the connection. To make assembly of the transtibial prosthetic easier in Sierra Leone, it is recommended to utilize the brass inserts rather than the locknuts due to a simplified printing process and the distribution of shear stress over multiple printing layers which complementarily might aid to complete a full dynamic test according to the ISO10328.



Chapter four

Influence of thickness, infill pattern and density on the flexural behavior of FDM printed tough PLA

Abstract

Introduction

Tough PLA is a new polymer for FDM printing with the similar material properties as PLA but with the hardness of ABS. Little research has been conducted about the flexural material properties of this material because it is relatively new. This study aimed to determine the flexural properties of tough PLA and establish a relation between infill pattern, density and thickness.

Method

Three point bending tests were performed in the Ametek Lloyd universal test machine with accordance to ASTM D790-17. Four types of tests were executed regarding infill pattern, percentages, thickness and material type. Maximum flexural stress, strain, flexural modulus and maximum load at failure were the main outcome measurements. Data was analyzed with MATLAB and for statistical analysis an one-way ANOVA tests were performed.

Results

Regarding infill pattern lines and grid were found most suitable for a transtibial socket. In general, the flexural strength increased with the density and thickness of the test specimens. However, the highest flexural stress was observed in samples with 70% infill. Those samples had a higher deflection before breaking due to more porosity, allowing a higher flexural stress. In addition, samples with the same thickness but different densities showed similar maximum loads, demonstrating that infill percentages in small samples does not add to the strength but the outer perimeter of the sample does.

Conclusion

Flexural strength is increased with the density and thickness. Since the outer perimeter contributed more to the strength of the test specimen than the infill itself, it might be possible to withstand the same force with less material. This is beneficial for producing the transtibial socket for amputees in third world countries since material costs could be further reduced while retaining the strength of the socket. The use of infill could potentially decrease the risk of failure of the patella region since crack propagation is counteracted by the air gaps in the internal structure. Establishing a design that adapts to the forces applied to the wall, could aid to create a thought out socket design with a more suitable density and thickness to prevent failure in the future.

4.1 Introduction

Bending tests are developed to investigate the flexural behavior of the materials. Through these tests flexural properties like flexural stress, strain and modulus could be determined⁶⁰. Knowing the bending properties of a material could aid analyzing if an object could endure certain loads. During a bending test, a test specimen is placed on two support. From above, a third support presses on the test specimen generating a load. The load causes the outer fiber of the specimen to stretch and the top fiber to compress⁶¹. Due to the elongation/contraction in combination with the applied load the material properties can be determined. Because three supports are used, this test is better known as the three point bending test (3PBT)⁶¹.

Two most used materials are polylactic acid (PLA) and Acrylonitrile butadiene styrene (ABS). PLA is a biodegradable polyester derived from renewable materials⁶². It is suitable for 3D printed objects with relative high details considering it is easy to print because PLA has the ability to heat and cool down without shrinking^{62,64}. Furthermore, PLA is especially suitable for biomedical applications because of its biocompatibility⁶². In contrast to PLA, ABS is a thermoplastic mainly used for applications where strength, ductility, machinability and thermal stability are needed⁶⁵. Ultimaker's tough PLA is a new type of PLA with the hardness of ABS. It is promised to have a higher impact resistance and therefore is preferable to use for functional applications such as molds, fixtures and tools⁶⁶. However, there is little literature regarding this material in relation to flexural properties, infill and thickness.

There are currently doubts about the strength of FDM printed sockets. As a result, sockets are printed more often by Selective Laser sintering (SLS)¹⁴. SLS uses a CO2 laser to fuse a layer of powdered polymer material¹⁹. This potentially creates a better adhesion between the layers and therefore a stronger design¹⁴. SLS is however more expensive than FDM and for that reason currently not suitable for aiding patients in developing countries²⁰.

Infill is the structure that fills up the space between the outer shells of a 3D printed object. A solid object is equal to 100% infill, it subsequently will use more material and take reasonably longer time to print. On the other hand, a 3D printed object with 0% infill with only thin outer shell would be inexpensive and quick to print. For many applications however this type of object would be impractical, as it would easily fail under the stress of normal usage. The infill density is directly correlated to the strength, weight and printing time. This relation does not increase linearly. For example, increasing infill percentage from 50% to 75% of PLA test specimens only results in an additional strength increase of 10%^{67,68,69}.

The pattern of the infill can affect the strength of the 3D printed object as well. There are many different shapes that can be printed. Cura⁷⁰, a slicing application for 3D printing, provides different 13 patterns. Pandzic et al⁶⁷ established that all infill patterns have a maximum ultimate tensile strength and yield strength with 90% infill for PLA. The highest ultimate tensile strength and yield strength was achieved with "Concentric" infill pattern with 90% infill, with only 15% reduction on ultimate tensile strength, 20% yield strength and 30% printing time in comparison to 100% infill^{64,65,66}. However, literature is not consistent. Other studies reported that Lines and honeycomb structure have higher tensile strengths than a concentric pattern⁶⁷. Because of the diversity of outcomes it is not clear which pattern has 'the best' properties.

Infill in 3D printing is always a compromise between strength on one hand and duration and costs on the other. For the transtibial socket it is therefore interesting to find out whether infill can maintain strength while using less material and at the same time reduce the risk of tearing. To our knowledge no literature is available regarding the bending properties of tough PLA in combination with infill settings. By means of, this study aimed to determine the flexural properties of tough PLA and establish a relation between infill pattern, density and thickness.

4.2 Method

4.2.1 test procedure

To investigate the relation between infill pattern, density and thickness three point bending tests are performed according to ASTM D790-17: Standard Test Methods for Flexural Properties of Unreinforced and Reinforced Plastics

Table 4-1: Print settings of the test specimens that were constant during all test

Material	Tough PLA
Printer	Ultimaker S5
Print temperature	225
Print speed	45 mm/sec
Nozzle size	0.8 AA
Bed temperature	60
Layer thickness	0.2 mm
Flowrate	1
Bottom layers	3
Top layers	3

and Electrical Insulating Materials⁷¹. The ASTM D790-17 test determines flexural properties of plastics by means of two support points and one load point (see page 36). All tests are executed in the Ametek Lloyd universal test machine. The test specimens were deflected until rupture occurred in the outer surface of the test specimen or until a maximum strain of 5.0 % was reached. A loadcell of 5000 N was utilized. The test specimens rested on support with a radius of 5 mm. The span length was determined by 1:16 of the total length of the test specimen. At mid-length of the span a third support was placed with a preload of 5 N. When a preload of 5 N was reached the deflection measurement system was set to zero. Then the test specimen was deflected with a constant rate depending on the thickness of the test specimen. The outcome measurements were flexural stress, strain, modulus and maximum load.

The flexural stress was calculated according to the following equation:

$$\sigma_f = \frac{3FL}{2hb^2} \quad (4-1)$$

Where

- σ_f = flexural stress [MPa]
- F = applied load [N]
- L = span [mm]
- B = width of the test specimen [mm]
- h = thickness of the test specimen [mm]

The flexural strain was calculated according to the following equation:

$$\varepsilon_f = \frac{600sh}{L^2} \% \quad (4-2)$$

where

- ε_f = flexural strain
- s = deflection [mm]
- h = thickness of the test specimen [mm]
- L = span [mm]

The flexural modulus was determined by the slope between $\varepsilon_{f1} = 0.0005$ and $\varepsilon_{f2} = 0.0025$ by:

$$E_f = \frac{\sigma_{f2} - \sigma_{f1}}{\varepsilon_{f2} - \varepsilon_{f1}} \quad (4-3)$$

The tests were subdivided in four stages. In each stage a specific feature was tested. Results of a previous stage determined the print settings of the test specimen of the next stage.

4.2.2 tests specimens

Three samples were printed in transversal and longitudinal direction for each test group (see figure 4-1). All print settings that were kept constant during the tests are summed up in table 4-1. These are the same print settings used for the initial transtibial socket. The test specimens were tested in an rectangular shape with the following dimensions: 127x25x6mm. Before testing the test specimen were measured according to the standard to ensure the dimension were accurately printed.

The test rates depended on the thickness of the specimen. When the standard thickness of 6 mm was tested, a test rate of 2.56 mm/min was set. The test rate of other thicknesses tested in test 3 was calculated by:

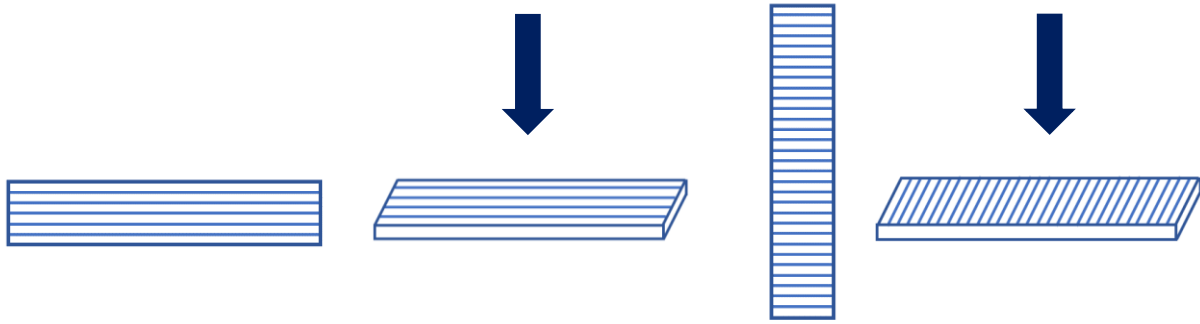


Figure 4-1: F.L.T.R. Front view of the direction of the test specimen when printed and the load direction during the 3PBT. The first so images show the longitudinal direction, the two on the right the transversal direction..

$$R = \frac{ZL^2}{6d} \quad (4-4)$$

Where:

R = rate of the crosshead motion [mm/min]

L = support span [mm]

d = thickness of the test specimen [mm]

Z = rate of straining of the outer fiber, z shall be equal to 0.01 [mm/mm/min]

4.2.3 infill pattern

During the first test, four infill patterns were tested: concentric, lines, grid and cubic subdivision (CS) (see figure 4-2). This study was conducted to investigate which pattern is most suitable for a transtibial prosthetic socket in terms of flexural strength. The patterns were tested with 60% and 80% infill except for the concentric infill. Currently the transtibial socket has 100% concentric infill. The golden standard throughout this study was therefore 100% concentric infill.

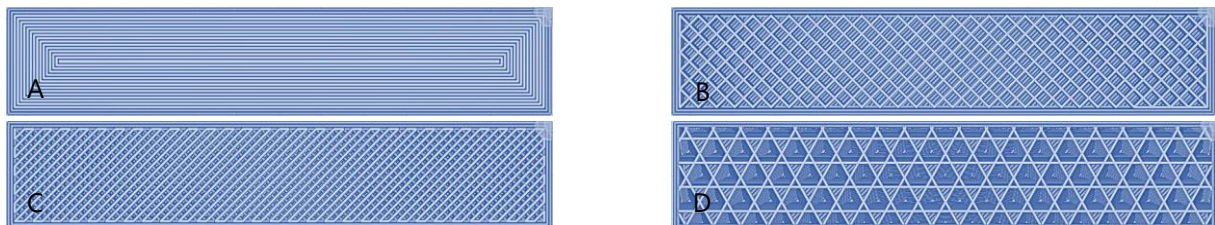


Figure 4-2: Mid-plane top view of longitudinal samples for different infill patterns. A: 100% concentric. B: 60% grid. C: 60% lines. D: 60% cubic subdivision.

4.2.4 Infill density

The second test was executed to determine the flexural strength of different infill percentages. The test was conducted with the infill pattern founded most suitable for the transtibial socket based on the test results of test 1. Again, 3PBT's were performed with the same dimensions as mentioned before in both transversal and longitudinal direction. All test conditions were kept the same.

4.2.5 Thickness

To investigated the influence of the thickness on the flexural strength, test 3 was performed. The infill pattern was fixed as the thickness and density were changed during these tests. The thickness varied from 4 mm to 12 mm with 2 mm intervals, the density varied from 30% to 90%. The infill pattern used in these tests was determined based on test 1 and 2. The main goal of this test is to establish a relation between density, thickness and flexural strength.

4.2.6 FDM versus SLS

To test whether the current used material is proportional to SLS 3D printed material, three points bending test were performed with polyamide 11 (PA11) and polyamide 12 (PA12) test specimens as well. The samples were printed with 100% infill in transversal and longitudinal direction by an external company named Oceanz. The results were compared to the 100% concentric infill tough PLA samples of test 1.

4.2.7 data analysis

Data was exported from the universal test machine as text files and analyzed in MATLAB version R2017B⁵⁶. In MATLAB the outcome measures were calculated and stress-strain curves were plotted. Statistical analysis was performed in SPSS version 25 software (SPSS Inc., Chicago, IL, USA). For statistical analysis an one-way ANOVA test was executed together with a test of homogeneity of variance. If the variance was equal a Turkey post hoc test was executed, if it was not equal a Games-Howell. Descriptive data were expressed in mean \pm standard deviation (SD). A p-value of <0.05 was considered as statistical significant

4.3 Results

4.3.1 Infill pattern

The results of the first bending tests are shown in appendix C table C-1. For the concentric infill plastic deformation occurred in all samples (see figure 4-3). Only one sample (T2) failed completely, two samples reached a strain of 5% (T2 and L1) and the tests were automatically stopped. The other three samples only the most outer fibers which endured the highest tensile forces broke (see figure 4-3A) The ASTM standard protocol specified if the specimen does not break or yield in the outer surface of the test specimen, the maximal flexural strength could not be determined. Figure 4-4 showed that the yield point is reached in all test samples, meaning that ultimate flexural strength could be determined. The flexural stress was approximately 80.08 MPa for transversal direction and longitudinal approximately 86.60 MPa.

All other test specimens failed during the 3PBT's with a strain $<5\%$. The transversal printed samples all broke mid-span while the longitudinal printed samples endured plastic deformation (see figure 4-3E). CS_{60%} was found substantial weaker than lines and grid in 3 out of the 4 cases, only longitudinal CS_{60%} versus lines_{60%} was found not significant ($P = 0.307$). For CS_{80%} only significant difference was found in transversal direction ($P=0.000$ vs lines, $P=0.000$ for grid). The CS pattern was withdrawn from further

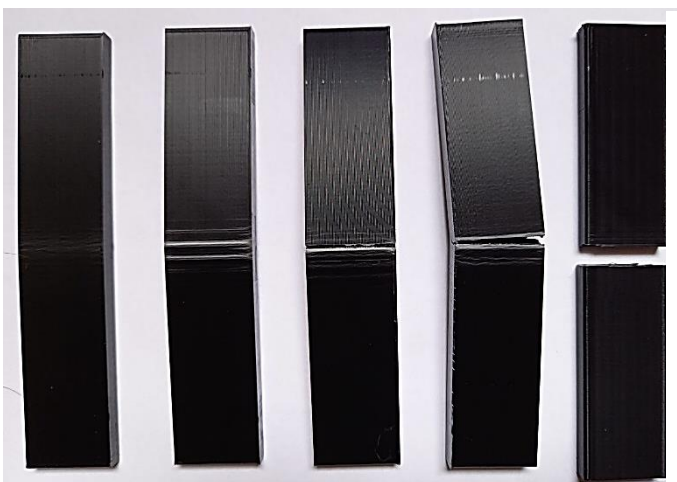


Figure 4-3: Types of failure: A: plastic deformation, B: stress line without tearing. C: stress lines with tearing. D: uneven failure can be recognized by the fact that a crack started at the edge and not in the middle. E: total failure mid-span

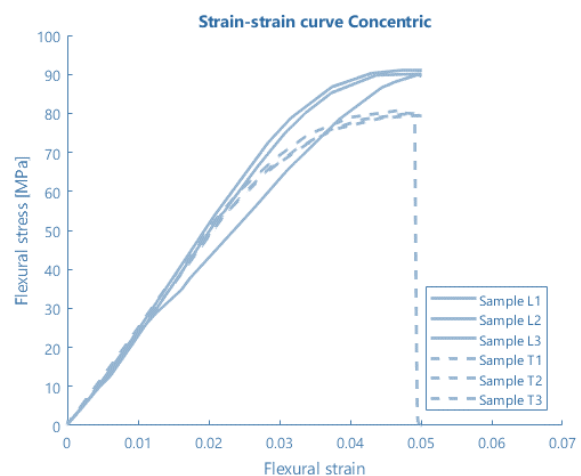


Figure 4-4: strain and strain curve of the concentric samples. T is transversal direction, L is longitudinal direction. Only one sample, L2 showed complete failure during this tests.

analysis due to the weaker flexural properties than the other patterns. The patterns lines and grid showed similar results between all samples but were found weaker than 100% concentric. Lines and grid were both included in the next test (see figure 4-5). The flexural modulus did not differ between longitudinal and transversal direction for all samples. In lower density samples a small decrease of the modulus was seen. This impact was however not significant

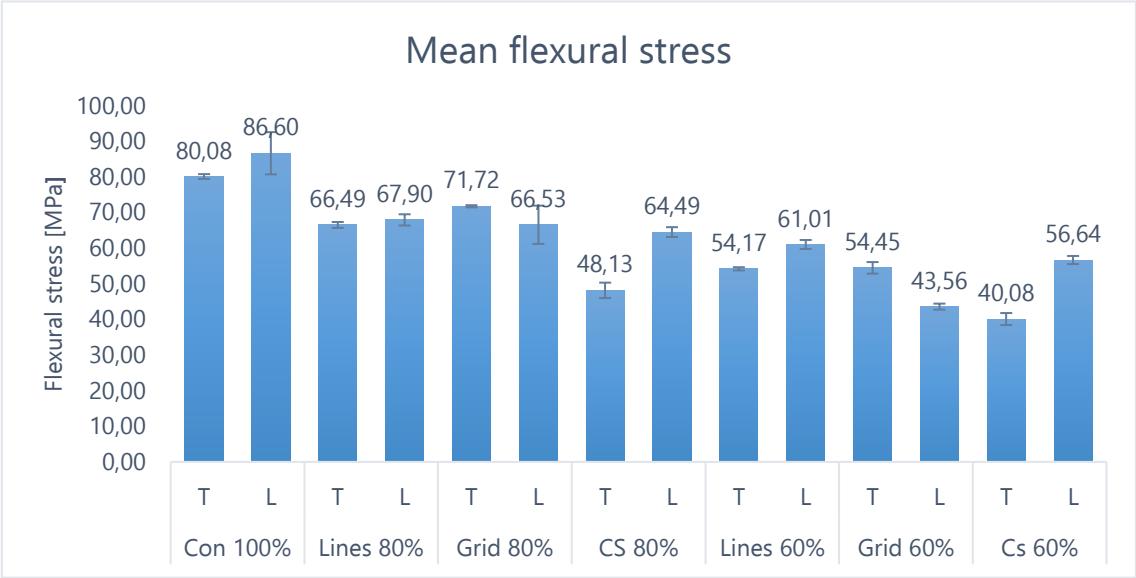


Figure 4-5: Mean flexural stress of test 1 for all samples with SD. Longitudinal direction was found stronger than transversal direction in most cases. CS shows weaker flexural stresses than lines and grid.

4.3.2 Infill density

The line and grid infill patterns were included in the second test because no decisive decision could be made as they showed similar results in test 1. During this test both infill pattern were tested with 50%, 70% and 90% infill (see appendix C table C-2). Again, results showed that all transversal specimens broke at mid-span while the longitudinal samples only endured plastic deformation or outer fiber failure with both strains <5%

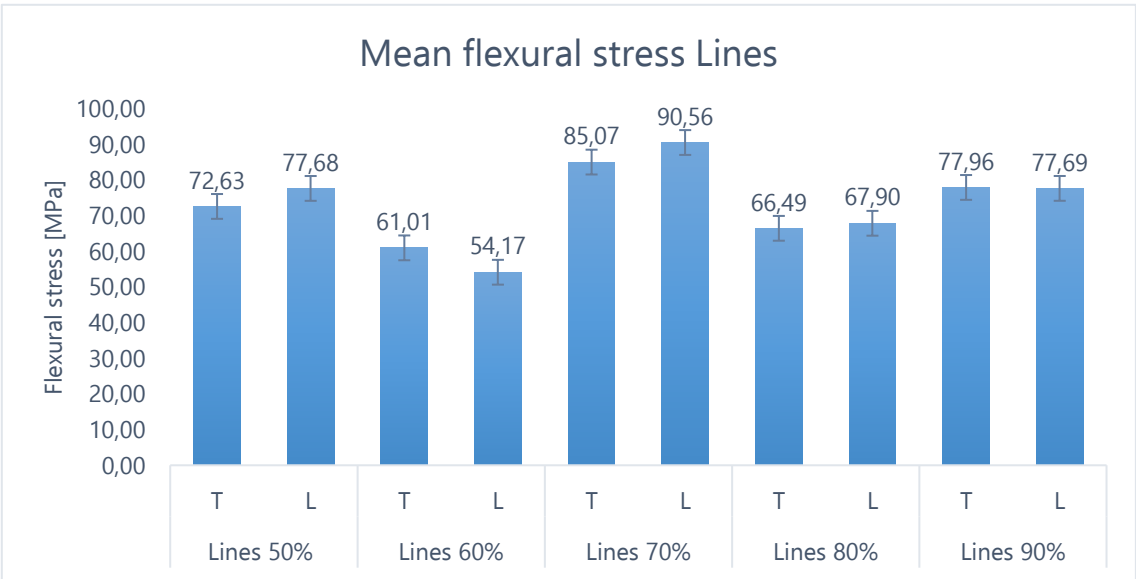


Figure 4-6: Mean flexural stress with SD of test 3 for the line pattern. Between longitudinal and transversal direction little difference was found, implying the pattern is strong in both direction. In addition, a decrease in stress is found in the 60% samples and an increase in 70% samples like the grid pattern

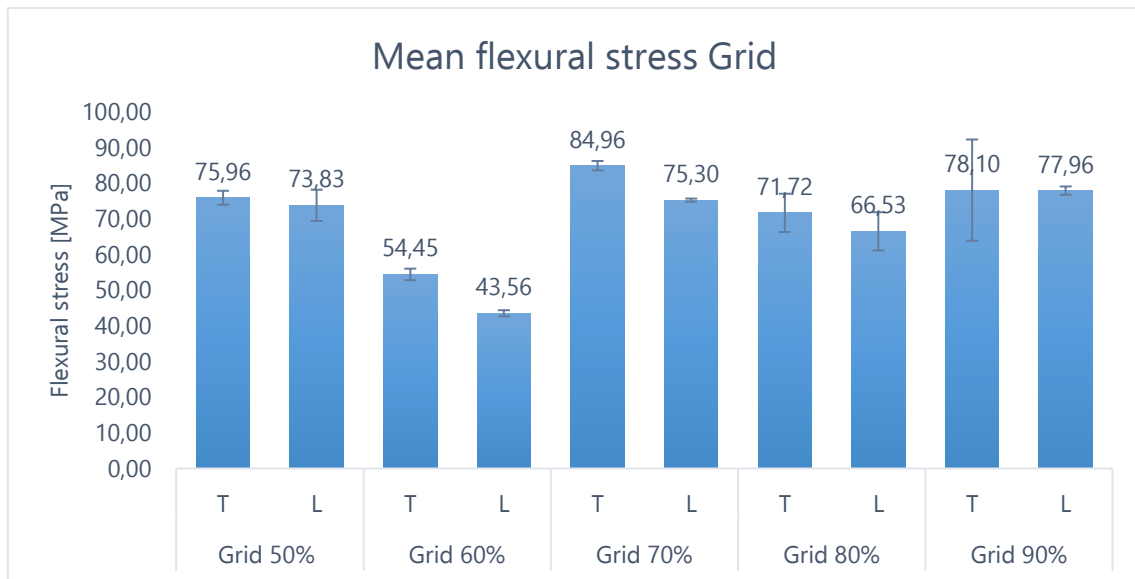


Figure 4-7: Mean flexural stress with SD of test 2 for the grid infill pattern. A decrease of stress is found in the 60% samples.

Figure 4-6 and 4-7 shows all average maximum flexural stress for both patterns including the test samples with 60% and 80% infill from test 1. For lines, lines_{70%} infill had the highest flexural stresses in both direction even compared to higher infill densities. This difference was more difficult to distinguish among the grid samples. Nevertheless both pattern at 70% had higher flexural stresses than concentric 100%. In general, higher stress were observed in the line pattern than grid. Between the samples with the highest flexural strength of lines_{70%}, was significantly higher than grid_{70%} in the longitudinal direction ($P=0.01$). So forth it was decided to continue the next test with the line pattern exclusively. Similar to test 1, no difference was found in flexural modulus during test 2. Comparing the flexural modulus of test 1 to test 2 showed however a substantial decrease. The same was observed with flexural stress, a decrease of flexural stress was seen with 60% and 80% infill compared to the samples of test 2.

4.3.3 Thickness

In test 3 the line pattern was tested with 30%, 50%, 70% and 90% infill and different thicknesses of the samples. The test rate was adjusted to the thickness to measure the accurate flexural stress. Figure 4-8 shows the average of maximum failure load of each sample group for both directions. A clear relation was establish: thicker samples could endure more load before breaking. But an equal thickness with a different infill percentages did not lead not a higher load, only a decrease of stress in within the sample as the thickness increased. Lastly, the flexural modulus decreased with the thickness of samples with the same infill density. Samples with the same thickness but other densities had similar flexural stresses (See appendix C table C-3).

Moreover, the amount of material is important to consider as well. It is logical that thicker test samples used more material. If it is established which forces an object must withstand, the most suitable composition can be chosen with the least use of material to make an optimum decision. For example: if an objects must endure 500 N in transversal direction, all samples from 8 mm to 12 mm thickness could endure this static load. In Cura (figure 4-9), slicing the simple socket design from chapter 2 with the same wall thickness of 8 mm but a different infill density (30% versus 90%), resulted in a decrease of 30% material and 5 hours of printing time. This led to a price reduction of €9.47, -. When lower material costs and printing times are required, like the prosthetic sockets for the patients in sierra leone, this a substantial reduction.

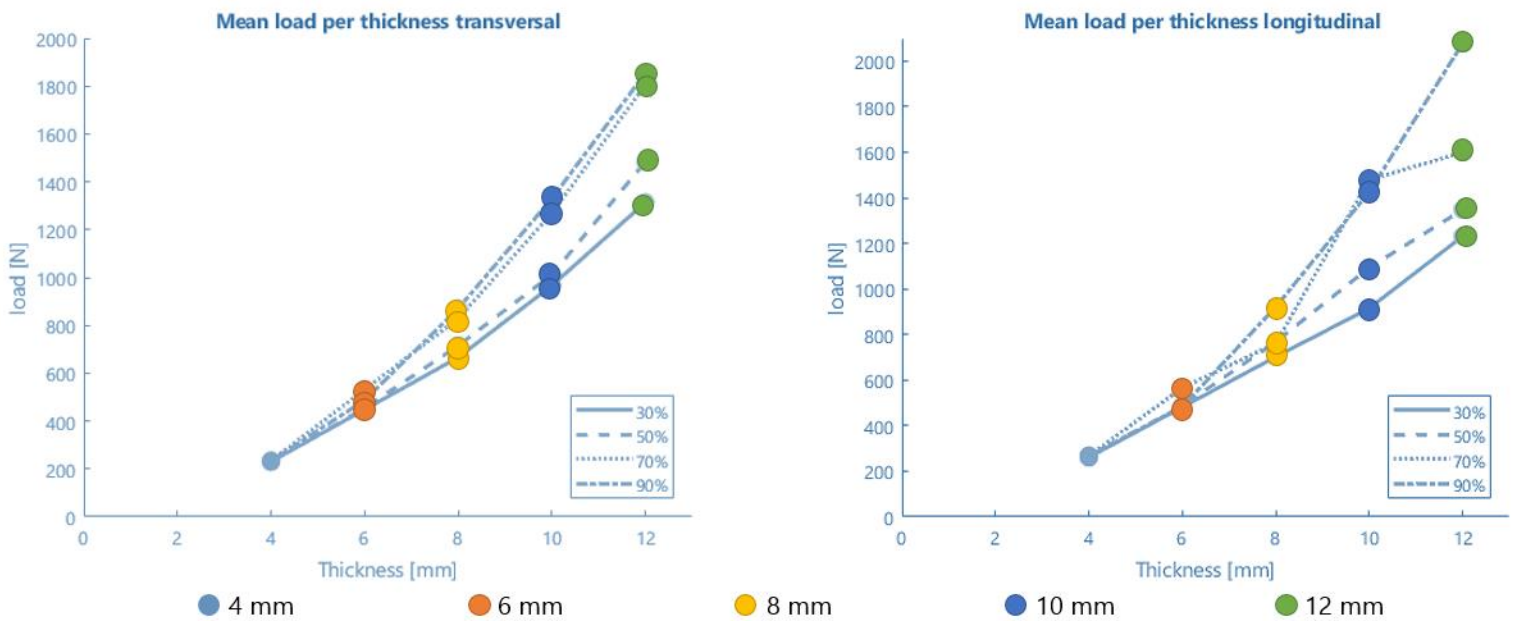


Figure 4-8: Mean values of flexural stress versus the load. Grey: 4 mm thickness, orange 6 mm thickness, yellow 8 mm thickness, blue 10 mm thickness and green 12 mm thickness. Thicker samples had higher loads to reach failure. However, an increase in density resulted in only higher flexural stresses.

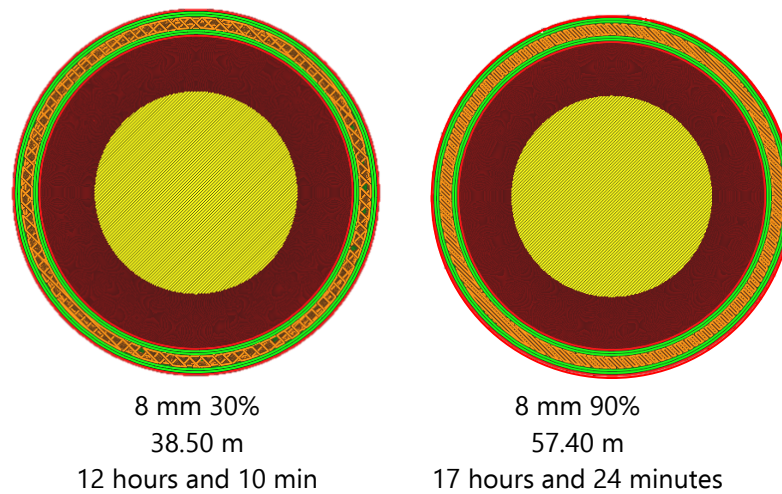


Figure 4-9: Mid plane view of sliced simplified socket in Cura with the same thickness but different infill percentages. A reduction of roughly 30% of material is seen and a decrease in printing time of approximately 5 hours.

4.3.4 FDM printed samples versus SLS printed

The SLS printed samples were tested under the same conditions as the tough PLA concentric_{100%}. Only one sample broke mid-span (PA11 T2). All other samples reached a strain of 5% and the test was automatically stopped. The PA12 samples however showed slight plastic deformation. The stress-strain curves of the PA11 and PA12 samples are showed in figure 4-10. These curves showed that PA12 reached the yield point as the curve flattens out after a linear elastic region. The PA11 samples showed no plastic deformation and did not reached the yield point, and therefore no maximum flexural stress could be determined. PA12 reached up to mean maximum flexural stress of ≈ 72.45 and ≈ 73.45 MPa for transversal and longitudinal respectively (see appendix C table C-4).

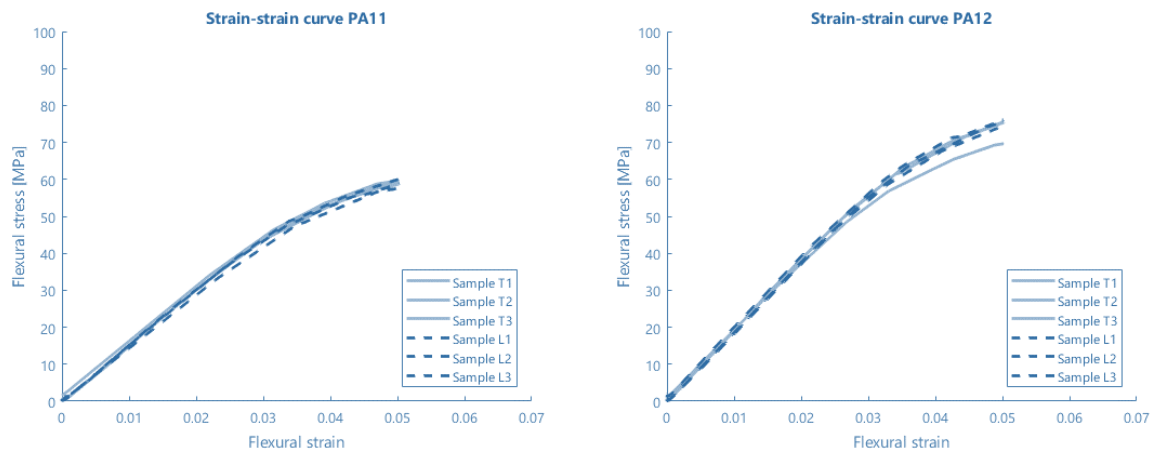


Figure 4-10: Stress-strain curve of PA11 and PA12. PA11 does not endure plastic deformation due to the flexibility of the material. PA12 does reach the yield point and plastic deformations occurred in the test samples.

4.4 Discussion

4.4.1 Infill pattern

For the concentric infill pattern only one sample broke completely, all other samples endured plastic deformation. Because the samples all reached the yield point according to figure 4.4, the average maximal flexural stress was determined for transversal and longitudinal of 80.06 MPa and 85.60 MPa respectively. The other infill patterns showed that transversal printed samples all completely failed at mid-span. Longitudinal specimens only endured plastic deformation. The infill pattern of the longitudinal samples is perpendicular to the applied load resulting to a denser structure. As a result, the applied load had to penetrate through more material creating more resistance to bending⁷³ (see figure 4-11) .

The CS pattern was found weaker than the other two patterns. The line pattern is printed by parallel diagonal lines in one print layer and opposite diagonals in the second layer, creating nodes where the diagonals cross. Within the grid pattern, the filament creates a framework that is deposited on top of each other. CS slightly shifts each print layer which results in fewer surface overlap between layers than the line and grid pattern, decreasing the adhesion and this is most likely the reason that this pattern was tested weaker.

4.4.2 infill percentages

In general, higher infill densities increased the flexural strength of an object. The increased density led to more surface overlap between print layers, increasing the node contact and inherently the adhesion⁶¹. A higher density provided a higher flexural modulus as well. As a result, higher densities samples behaved more rigid than samples with lower percentages of infill, making them more resilient. However, results showed that 70% infill was relatively higher in flexural strength than 80% and 90% infill for the line pattern. Because of higher porosity of lines^{70%} allowed more deflection before failure. The more flexible behavior of 70% infill samples might explain the higher flexural stresses.

In addition, the quality of samples depended on several factors during the printing process. First of all 3D printed objects are heterogeneous, allowing them to behave differently between sample groups. This is demonstrated for example with the Tgrid_{90%} samples whereas one of the samples only reached a flexural stress of 61.71 MPa. This difference in behavior makes it hard to accurately determine the material properties with small sample sizes.

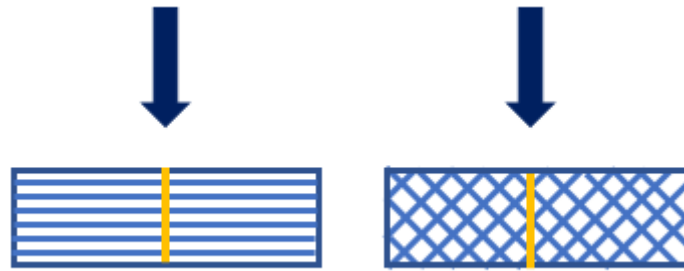


Figure 4-11: A cross-section of a longitudinal printed sample (Left) versus a transversal printed sample (right). Longitudinal stacks the pattern on top of each other creating a denser structure perpendicular to the load.

Another noticeable phenomenon which was not in line with the literature was the decrease of flexural stress of 60% and 80% samples compared to the samples of the second test. This is likely explainable by the fact it was printed in another batch than the samples of test 2. Changes during the printing process or to the building platform have possibly occurred causing the results to differ from the second test.

4.4.3 Thickness

This test showed a proportional relationship between the thickness and tolerable load. Samples that were thicker could bear more load. Samples with the same thickness but other density showed that they could endure roughly the same load, but developed more stress within the test sample. As a result, it is possible to withstand the same force with less material.

Establishing that samples with the same thicknesses could endure the same load with lower densities, helps to better determine which composition is needed for the transtibial socket in the future. Ideally, it is precisely mapped out which forces are present in the wall of the socket in order to choose the correct thickness and density for a specific area. This might lead to overall reduction of costs and printing time.

However, shell thickness might have played an important role in terms of strength as well. Shells are the outer perimeter of layers of a 3D printed object. Because the thickness of the test samples were relatively thin, the ratio of density and shell thickness might have an additional contribution to the strength. The effect of shell thickness is yet to be determined.

4.4.4 FDM printed samples versus SLS printed

The stress-strain curve of the SLS printed samples showed that PA12 samples reached the yield point and endured plastic deformation, and therefore can be compared to the golden standard samples of concentric_{100%}. The concentric samples had greater flexural stresses in both directions, this demonstrated that FDM printed material is not inferior to SLS printed material in terms of flexural properties. The maximum flexural stress of PA11 however could not be determined and therefore no comparison could be made.

Oceanz performed tensile test according to the ISO527⁷³ with PA11 to determine the maximum tensile strength. Van der stelt et al²¹ performed the same tests with tough PLA. PA11 showed a maximum tensile strength in x and y direction of 45.5 MPa and 45.68 MPa respectively⁷⁴. The maximum tensile strength of tough PLA was determined to be 47.2 MPa in longitudinal direction and 27.9 MPa transversal direction²¹. Because SLS objects are made from power fusion, the print direction had no influence on the strength of the object. Nevertheless, this effect can be observed with FDM, where an object is stronger if the force is applied along the printing direction. Comparing PA11 to tough PLA showed that in longitudinal direction the materials are equally strong. In transversal direction, the

adhesion between the layers of the tough PLA test specimens felt short and is substantial weaker than the PA11.

Nevertheless, FDM has some advantages over SLS. Because SLS is a powder based printing method, only solid objects can be printed⁷. FDM can print with infill and as shown in this study could result in stronger samples with less material and printing time. Furthermore, SLS printed parts may endure shrinkage and warpage due to sintering and cooling which might result in a less accurate design²⁰. Lastly, FDM can print with high accuracy, costs less and has faster printing speeds making this AM technique suitable for the production of 3D printed transtibial sockets in rural areas²⁰.

4.4.5 Limitations

This study has some limitations. First of all, a small sample size was used. If outlier in a sample group was present, a large standard deviation was the outcome. Which could give a biased view of the strength of a sample composition. To reduce the standard deviation and error, a larger sample size can be used in order to determine flexural properties more accurately.

The outliers indicated the difference in material behaviour of a sample group as well. This is supported by that not all samples failed the same. A few samples broke at an angle due to the heterogeneity of the material. Other samples failed at the edge tearing to the middle of the sample instead of a tear started in the middle and lacerated evenly to the outer edges (see figure 4-3D). The unevenly broken samples implied that stress concentrations had emerged at the edge. This was attributed to the fact that a brim that was added by the printer when the samples were printed. This brim was removed before testing but a small remnant of this brim could cause unevenness on the edge of the sample. The remnant could induce a stress concentration, causing the sample to break unevenly. Luckily, that effect was only seen in 2 samples.

Lastly, these test only investigated the flexural behaviour of test samples and not a whole prosthetic socket. Testing a complete socket might derive other results since the forces are not only applied perpendicular to the socket. In addition, now only a static load is applied until maximal failure and in reality a repetitive load acts which eventually led to failure of the socket. This research however gains information about what load can be applied to a specific composition until it fails. This will aid to make a thought out socket design in which a more suitable density and thickness are used to prevent failure of the socket in the future. However, only tests with a 3D printed socket tested dynamically according to the ISO10328 and long-term outcomes will reveal whether changes the infill pattern, density or wall thickness will lead to a more sustainable socket.

4.6 Conclusion

In conclusion, this study aimed to provide the flexural properties of tough PLA and establish a relation between infill pattern, density and thickness. Overall, flexural strength is increased with the density and thickness. This is due to an increase of flexural modulus and a greater second moment of inertia. However, samples with the same thickness but other density showed that they could endure roughly the same load because the flexural strength of a object come from the outer perimeters and not the middle part. As a result, it might be possible to withstand the same force with less material. This is beneficial for producing the transtibial socket for amputees in third world countries since material costs could be further reduced. Furthermore, this contributes to a better understanding of the flexural behaviour of tough PLA in different compositions. Which helps to create a thought out socket design in which a more suitable density and thickness could be used to prevent failure. Hopefully this will provide a more sustainable 3D printed transtibial socket for the amputees in developing countries.



3D Sierra Leone 2020, Merel van der Stelt

5.1 General discussion

In the beginning of this thesis questions were defined. The sub questions led to an overall answer of the main research question. In this chapter the sub questions are briefly answered and recommendations were written for further research.

5.2 Sub questions

5.2.1 What are the fragile parts of the current socket design?

The dynamic test of the ISO10328 revealed a weak spot in terms of adhesion on the print layer where the locknuts are located. These locknuts are used for the assembly of the socket to the pylon. The use of locknuts results in stress accumulations on this print layer. When a repetitive load is applied to this part, the compression and tensile forces presumably have resulted in micro tears which eventually led to failure of this part during the test.

Other weak spots were identified by the long-term outcomes of daily usage by patients in Sierra Leone. In two of the eight cases a tear developed in the patella region perpendicular to the print direction. In one case the tear propagated between the print layers to the right condyle cap, which led to detachment of the condyle cap. Finite element analysis showed stress accumulations in the patella region and the back corners of the condyle because of the geometry of the socket and forces that are applied during gait and contact pressures between the socket and residual limb.

5.2.2 What are the problems regarding the assembly of the 3D printed transtibial prosthetic?

Apart from being a vulnerable point, the second problem regarding the use of locknuts is that it is quite impractical. To embed the locknuts into the socket, the printer has to be paused after approximately four hours of printing. Then the locknuts are placed in the prior designed pockets. However, the locknuts does not always fit properly. Then they have to be heated and pushed into the pockets. To simplify the printing process this thesis investigated the possibilities of other assembly methods

5.2.3 What are the possibilities to strengthen the fragile parts?

First, this thesis conducted research for other methods to assembly the socket to the pylon. Three assemblies were tested and it was concluded that brass inserts have a high possibility to overcome the disadvantages regarding the use of locknuts. The main benefit of inserts is that they are melted into a prior designed screw hole increasing the adhesion of layers around it. The increase of surface between the assembly and material of the socket will subsequently divide the stress over a larger area, decreasing the stress accumulations over multiple print layers. Those benefits potentially contribute to complete the dynamic test of ISO10328.

Secondly, to strengthen the patella and condyle caps the overall wall thickness could be simply increased. But it subsequently will lead to an increase in printing time and material costs. Partially increase of the wall thickness around the patella and condyle caps contribute to less printing time and materials costs however not resulted in more division of the stress accumulations found with the finite element analyses. The scope of this thesis was to investigate the influence of infill density and pattern in order to reduce material costs while retaining the strength and reduce the chance of tearing.

5.2.4 Is it possible to use less material in order to reduce the costs even further while retaining the strength?

This thesis showed it is possible to use less material by the means of infill. The use of infill does not lead to loss of strength since the outer perimeters of an object contribute more to the strength than the middle part. The sockets in Sierra Leone failed because a crack occurred at the outer perimeter and propagated through the socket wall. The use of infill might make it more difficult for a crack to

propagate because of the air pockets between the material. As a result, a crack cannot tear completely at once. In addition, lower infill percentages decrease the flexural modulus creating a more flexible object as well. This flexibility allows more deflection before failure. The proper combination of shell thickness and infill percentage will be calculated based on an analytical model. The collected data from this thesis will be used to compute where in the socket certain forces are at play and which shell thickness and infill percentage is needed to counteract those forces. Therefore, in the future the socket is hopefully more sustainable with the use of less material.

5.3 Future recommendations

In this section first the main findings of this thesis are discussed. Afterwards, various ideas for further research and strengthening the current design are proposed.

5.3.1 Main findings

In the future it is recommended to avoid strong geometrical changes in the overall design. This can be accomplished with flattening out the back part of the popliteal depression. In addition, it might be possible to make the condyle caps less high in order to achieve smoother transition between the front/back of the socket and the condyle caps (see figure 5-1). The dimensions of initial design were based on the conventional method of socket manufacturing. Recently, smaller condyle caps are observed in the conventional method. The main reason is that the condyle caps might contribute less to the stability than previously predicted. Reduction in size of the caps potentially results to less stress since the transition from the patella to the caps and from the caps to the popliteal depression is more gradual.

Secondly, for the assembly of the socket and pylon it is advised to switch to brass inserts instead of locknuts. This thesis showed that in term of torque-out and pull-out strength the brass insert is not inferior to the locknuts. The main advantage of the use of inserts is that the plausibly increases the adhesion around the assembly, simplified the printing and assembly process and divide the stress over a greater surface. Altogether, this might contribute to accomplishing a full dynamic test and gives future perspective to produce the socket in the Netherlands as well.

Lastly, this thesis investigated the influence of infill pattern, density and wall thickness. A database was created with the strengths of all types of different compositions. The concept is to use this database to create a more thought out and sustainable design. An analytic model will be created that will accommodate a more detailed FEA. This model will reveal the best composition of different parameter (density, shells, thickness) in order to establish enough strength to withstand specific loads. And on the other hand, to decrease material costs and printing time as much as possible. In the end this research will contribute to create a more sustainable design in such manner that the patients in Sierra Leone could longer benefit from their prosthetic.

5.3.2 Gradient infill

When an object is loaded, the stresses are the highest in the outer perimeters and zero in the middle. Recently, researchers are experimenting with gradient infill. This type of infill creates a higher infill density at the outer perimeters of the object and a lower the infill density in the middle of the structure⁷⁵. As a result, the outer parts that endure more load are made stronger as the strength of an object increases with the infill

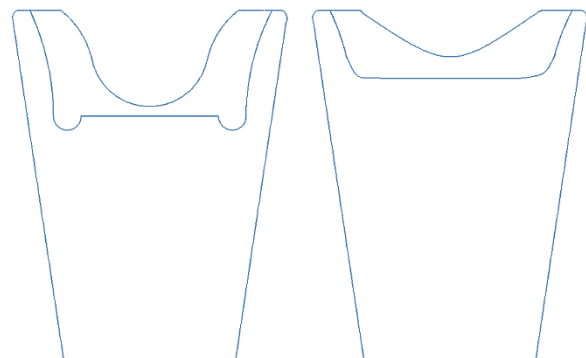


Figure 5-1: example for smoother transition between the back/front and condyle caps. Smaller condyle and flattening the popliteal depression.

density. This gradient infill can be coded and imported in Cura. If the forces on the socket are mapped out, the most suitable infill can be incorporated in a specific area by means of coding. Making the design of the socket stronger at areas that need it and use less material on areas that not have to withstand large loads. This step can potentially be included in the design reducing the material costs even further.

5.3.3 Cooling

Cooling the material after it has been deposited is necessary for parts with high accuracy. However, for functional parts cooling might be less necessary since as the cooling rate increase, the tensile strength for both directions is decreased. A higher cooling temperature is related to emerge of voids and less overlap between the print layers decreasing the adhesion between layers. Contrarily, lower cooling temperatures could lead to warping of the material⁷⁶. Currently the sockets are printed with a 100% cooling rate. Since the functionality of the socket is more important the millimeter accuracy, it might be interesting to find out whether decreasing the cooling rate could add to the strength of the socket. Especially, if the interlayer adhesion is increased this might be extra beneficial for the dynamic tests.

5.3.4 Extrusion width

The extrusion width defines how wide the filament is printed and sets the distance between extruded filaments. When the extrusion width is set higher than the nozzle size, more pressure is generated inside the nozzle, this pressure will not only increase the width of the filament but presses the filament harder to other layers. In theory this should increase the adhesion and therefore the strength. For example, tests with PLA showed that objects with twice the extrusion width could bare almost double the load until failure⁷⁷. Again, increasing the extrusion width will automatically lead to less detail, but to a certain extent this is not critical for the socket.

5.3.5 Layer height

The layer height determines the accuracy of a print in vertical direction. A lower layer height typically results in parts with a smoother surface but it automatically takes a longer time to print. Some literature states that lower layer height creates stronger designs as the fusion between layers is improved. Due to the low distance between the nozzle and the building platform, the previous layer is heated as well as the new layer of filament and this helps with bonding. In addition, smaller gaps are formed between layers creating a denser structure⁷⁸. On the other hand, a greater layer height creates less layers in total throughout the design. This makes the chance of failure between printing layers less, better known as statistical size effect⁷⁹. The rule of thumb is not to extend over 80% of the nozzle size. Studying the effect of layer height might aid to gain insight which layer height makes the strongest composition. Afterwards, this could be cooperated into the socket design.

5.3.6 Post processing steps

Lastly, some postprocessing steps could improve the adhesion as well. One of those methods is annealing. Van der Stelt et al⁸⁰ investigated this process for tough PLA is and it was concluded that it had no added value for the strength of tough PLA⁸⁰. However, one new way of annealing was not tested: annealing with salt.

Remelting 3D prints in salt is a new method of post processing where the printed parts are embedded into powder salt and afterwards placed inside an oven. It is suggested that this heating process will increase the crystallinity of the material and therefore the strength⁸⁰. The first studies with PLA showed samples that were remelted with salt had less porosity and a more homogenic inside structure⁸¹. As a result, the tensile strength was substantially improved. This method is quite simple and applicable in Sierra Leone. However, this method can only be used with parts that are solid. If the shift is made to print the socket with infill in the future, then this method will not be suitable.

Vapor smoothing is a post processing method which uses acetone to dissolve the outer layer of a 3D printed object. This dissolvment results in a smooth surface as well as a better adhesion of the perimeters throughout the whole design.. It is relatively an easy process but acetone is highly flammable and toxic if it is inhaled too much. Therefore, the process must be carried out carefully and is more difficult than an annealing process.

5.4 Final conclusion

This thesis conducted research about how to improve the strength and sustainability of an FDM 3D printed transtibial prosthetic socket for patients in Sierra Leone. As one can conclude, there are many possibilities to achieve this. The scope of this review was to investigated other methods to assemble the socket to the pylon and if the use of different printer settings (infill density, pattern and thickness) could improve/retain the strength but decrease the material costs at the same time. This thesis demonstrated that the use of brass inserts had more advantages over the use of locknuts. Brass inserts simplified the printing process and could potentially aid to complete a full dynamic test of the ISO10328. Moreover, the use of infill could reduce the material costs while retaining the strength of the socket. Collectively, this hopefully contributes to improve the life span of the socket so the patients in Sierra leone could benefit of the prosthetic of a longer period of time. This inherently improves the quality of life for those patients because they are able to participate in society.

At last, this thesis ended with future possibilities to strengthening the socket design that could still be research. Research about the use and improvement of FDM in many different areas is published very frequently. Therefore, it is important to be mindful and up-to-date of new developments in this field, as it might be the solutions regarding problems in the future.

References

- [1] Marino M. *et al.*, "Access to prosthetic devices in developing countries: Pathways and challenges," *2015 IEEE Global Humanitarian Technology Conference (GHTC)*, Seattle, WA, USA, 2015, pp. 45-51, doi: 10.1109/GHTC.2015.7343953.
- [2] Van der Stelt M, Grobusch M.P, Papenburg M, Slump C.H, Maal T.J.J, Brouwers L. "Short-term follow-up of low-cost 3D-printed transtibial prosthetics in a rural area of Sierra Leone". Tech. rep. *University of Twente*, June 2020.
- [3] World health organization. (2015, september). Standards for prosthetics and orthotics service provision (Nr. 4). [https://www.who.int/phi/implementation/assistive technology/workplan_p-o standards.pdf](https://www.who.int/phi/implementation/assistive%20technology/workplan_p-o_standards.pdf)
- [4] Matter R, Harniss M, Oderud T, Borg J, Eide AH. Assistive technology in resource-limited environments: a scoping review. *Disabil Rehabil Assist Technol*. 2017 Feb;12(2):105-114. doi: 10.1080/17483107.2016.1188170. Epub 2016 Jul 21. PMID: 27443790.
- [5] van der Stelt M, Verhulst AC, Vas Nunes JH, Koroma TAR, Nolet WWE, Slump CH, Grobusch MP, Maal TJJ, Brouwers L. Improving Lives in Three Dimensions: The Feasibility of 3D Printing for Creating Personalized Medical Aids in a Rural Area of Sierra Leone. *Am J Trop Med Hyg*. 2020 Apr;102(4):905-909. doi: 10.4269/ajtmh.19-0359.
- [6] Worlddata, "Average income around the world 2018," 2018. [Online]. Available: <https://www.worlddata.info/africa/sierra-leone/economy.php>. [Accessed: 14-Jan-2021].
- [7] Aherwar A, Signh A, Patnaik A. A Review Paper on Rapid Prototyping and Rapid Tooling Techniques for Fabrication of Prosthetic. *High Value Manufacturing ADVANCED RESEARCH IN VIRTUAL AND RAPID PROTOTYPING* (2013). DOI: 10.1201/b15961-64
- [8] Quinlan J. "Estimating the prevalence of limb loss in the United States: 2005 to 2050." *Arch Phys Med Rehabil* (2008), 89(3), 422–429. DOI: 10.1016/j.apmr.2007.11.005.
- [9] Nurhanisah MH, Jawaid M, Ahmad Azmeer R, Paridah MT. The AirCirc: design and development of a thermal management prototype device for below-knee prosthesis leg socket. *Disabil Rehabil Assist Technol*. 2019 Jul;14(5):513-520. doi: 10.1080/17483107.2018.1479782. Epub 2018 Jun 22. PMID: 29933703.
- [10] Tay, F.E.H., Manna, M.A. and Liu, L.X. (2002), "A CASD/CASM method for prosthetic socket fabrication using the FDM technology", *Rapid Prototyping Journal*, Vol. 8 No. 4, pp. 258-262. <https://doi.org/10.1108/13552540210441175>
- [11] Wan Fadzil WFA Mazlan MA. "3D printed lowerlimb socket for prosthetic legs". *IJERN* (2019), 6(3), 2349–2058.
- [12] Sengeh DM, Hugh H. "A Variable-Impedance Prosthetic Socket for a Transtibial Amputee Designed from Magnetic Resonance Imaging Data". *Journal of Prosthetics and Orthotics*. (2013), 25(3), 129–137. DOI: 10.1097/JPO.0b013e31829be19c.
- [13] Ng, P., Lee, P.S.V., Goh, J.C.H. (2002). Prosthetic sockets fabrication using rapid prototyping technology. *Rapid Prototyping Journal* 8 (1) : 53-59. ScholarBank@NUS Repository. <https://doi.org/10.1108/13552540210413310>
- [14] Simpson D, Herbert N. "A preliminary investigation into the development of 3-D printing of prosthetic sockets." *J Rehabil Res Dev*. (2005), 42(2), 141–146. DOI:10.1682/jrdd.2004.08.134
- [15] Fang L, Jia X, Wang R. Modeling and simulation of muscle forces of trans-tibial amputee to study effect of prosthetic alignment. *Clin Biomech (Bristol, Avon)*. (2007 Dec);22(10):1125-31. doi: 10.1016/j.clinbiomech.2007.07.017.
- [16] Stenvall E, Flodberg G, Pettersson H, Hellberg K, Hermansson L, Wallin M, Yang L. Additive Manufacturing of Prostheses Using Forest-Based Composites. *Bioengineering*. 2020; 7(3):103. <https://doi.org/10.3390/bioengineering7030103>
- [17] Abbady HEMA *et al.* 3D-printed prostheses compared with non-3D-printed prostheses in developing countries: a systematic review. *Radboud University Medical Center, Nijmegen, the Netherlands*, July 2020.

- [18] Attaran M. "The rise of 3-D printing: The advantages of additive manufacturing over traditional manufacturing". *Business Horizons*. (2017), 60(5), 677–688. DOI: 10.1016/j.bushor.2017.05.011.
- [19] Mohamed et al. "Optimization of fused deposition modeling process parameters: a review of current research and future prospects". *Adv. Manuf.* (2015), 3,42–53 DOI 10.1007/s40436-014-0097-7
- [20] Sandeep, Chhabra D. 2017. "Comparison and analysis of different 3D printing techniques." *IJLTET*, 8(4-1). Aug pp. 264-272
- [21] van der Stelt M, Verhamme L, Slump C.H, L. Brouwers L, Maal T.J.J. Strength testing of low-cost 3D-printed transtibial prosthetic socket *University of Twente, Radboud UMC*. June 2020.
- [22] European committee for standardization, "Nen-en-iso 10328," 2016.
- [23] Brenner, S., & Scott, L. R. (2013). *The Mathematical Theory of Finite Element Methods* (3de editie). Springer Publishing..
- [24] Jamaludin MS, Hanafusa A, Shinichirou Y, Agarie Y, Otsuka H, Ohnishi K. Analysis of Pressure Distribution in Transfemoral Prosthetic Socket for Prefabrication Evaluation via the Finite Element Method. *Bioengineering* (Basel). 2019 Oct 24;6(4):98. doi: 10.3390/bioengineering6040098. PMID: 31652967; PMCID: PMC6956391.
- [25] Ali I. Kumar R. Singh Y. Finite Element Modelling and Analysis of Trans-Tibial Prosthetic Socket. *Global journal of Researches in Engineering*. 2014. 14(4);42-50
- [26] Hibbeler RC. (2006) *Sterkteleer*. Pearson education
- [27] Dr.ir. Langelaar M. 9 nov 2020. *Sterkteleer – spanning* [powerpoint]
- [28] Dr.ir. Langelaar M. 11 nov 2020. *Sterkteleer – rek* [powerpoint]
- [29] Dr.ir. Langelaar M. 18 nov 2020. *Sterkteleer – Buiging* [powerpoint]
- [30] Cuellar Lopez J.S. (2021) *Accessible Hand prostheses: 3D printers meet smarthphones*. University of Technology Delft, Faculty of Werktuigbouwkunde, Maritieme Techniek & Technische Materiaalwetenschappen
- [31] Afrose, M.F., Masood, S.H., Iovenitti, P. et al. Effects of part build orientations on fatigue behaviour of FDM-processed PLA material. *Prog Addit Manuf* 1, 21–28 (2016). <https://doi.org/10.1007/s40964-015-0002-3>
- [32] Jia X, Zhang M, Lee WC. Load transfer mechanics between trans-tibial prosthetic socket and residual limb--dynamic effects. *J Biomech*. 2004 Sep;37(9):1371-7. doi: 10.1016/j.jbiomech.2003.12.024. PMID: 15275844.
- [33] Ten cate, W., May 2017. "Prosthetic Socket Design for Fused Deposition Modeling.". MS Thesis, University of Technology Delft, Faculty of industrial design,
- [34] Van sitteren, M. 2016. "A new 3D printed Volume Adaptive Prosthetic Socket for below-the-knee amputees". MS Thesis, University of Technology Delft, Faculty of industrial design,
- [35] Laing S, Lee PV, Goh JCh. Engineering a trans-tibial prosthetic socket for the lower limb amputee. *Ann Acad Med Singap*. 2011 May;40(5):252-9. PMID: 21678017.
- [36] Goh JCH et al. Static and dynamic pressure profiles of a patellar-tendon-bearing (PTB) socket. *Proceedings of the Institution of Mechanical Engineers, Part H: Journal of Engineering in Medicine*. 2003;217(2):121-126. doi:10.1243/09544110360579330
- [37] Ali, I et al (2014). Finite Element Modelling and Analysis of Trans-tibial Prosthetic Socket. *Global Journal of Research In Engineering*, 14.
- [38] Faustini et al. "The quasi-static response of compliant prosthetic sockets for transtibial amputees using finite element methods" *Medical Engineering & Physics*, 06 Jun 2005, 28(2):114-121 DOI: 10.1016/j.medengphy.2005.04.019

- [39] Zhang M, Lord M, Turner-Smith AR, Roberts VC. Development of a non-linear finite element modelling of the below-knee prosthetic socket interface. *Med Eng Phys*. 1995 Dec;17(8):559-66. doi: 10.1016/1350-4533(95)00002-5. PMID: 8564149.
- [40] Zachariah SG, Sanders JE. Interface mechanics in lower-limb external prosthetics: a review of finite element models. *IEEE Trans Rehabil Eng*. 1996 Dec;4(4):288-302. doi: 10.1109/86.547930. PMID: 8973955.
- [41] Solidworks (Version 2020-2021). (1995).Dassault Systèmes.Datasheet tough PLA
- [42] Technical data sheet Tough PLA. Version 1,002. Ultimaker. Sep (2018). [online] available: <https://support.ultimaker.com/hc/en-us/articles/360012759599-Ultimaker-Tough-PLA-TDS>
- [43] Dumbleton T, Buis AW, McFadyen A, McHugh BF, McKay G, Murray KD, Sexton S. Dynamic interface pressure distributions of two transtibial prosthetic socket concepts. *J Rehabil Res Dev*. 2009;46(3):405-15. PMID: 19675992.
- [44] Hubregtse F, Cremers, F. Bosch S. (2020). D4AM Sierra Leone Contains the design proces of the socket and cover from start to finish. University of applied sciences.
- [45] Wittel H, Muhs D, Jannasch D, Vobiek J. (2016) Rollof/Matek machineonderdelen Tabellenboek. Amsterdam : Boom.
- [46] Saey T. "Evaluation of the influence of cyclic loading on a laser sintered transtibial prosthetic socket using Digital Image Correlation (DIC)". *Conf Proc IEEE Eng Med Biol Soc*. (2019), 5382–5385. DOI: 10.1109/EMBC.2019.8856544.
- [47] LH. Hsu, GF.Huang, C. L. D. S. L., 2010. "The development of a rapid prototyping prosthetic socket coated with a resin layer for transtibial amputees.". *Prosthet Orthot Int*, 34(1), Mar, pp. 37–45.
- [48] E.L. Doubrovski, E.Y. Tsai, D. D. J. G. H. H. N. O., 2015. "Voxel-based fabrication through material property mapping: A design method for bitmap printing". *Computer-Aided Design*, 60, pp. 3–13.
- [49] C. Comotti, D. Regazzoni, C. R. C. A. V., 2015. "Multi-material design and 3d printing method of lower limb pros-thetic sockets". In *Proceedings of the 3rd 2015 Workshop on ICTs for Improving Patients Rehabilitation Research Techniques, REHAB '15*, Association for Computing Machinery, p. 42–45.
- [50] Wasti S, Adhikari S. Use of Biomaterials for 3D Printing by Fused Deposition Modeling Technique: A Review. *Front Chem*. 2020 May 7;8:315. doi: 10.3389/fchem.2020.00315. PMID: 32457867; PMCID: PMC7221194.
- [51] Rahim TNAT, Abdullah AM, Akil HDM. Recent Developments in Fused Deposition Modeling-Based 3D Printing of Polymers and Their Composites. *Polymer Reviews*. 2019 59(4): 589-624, DOI: 10.1080/15583724.2019.1597883
- [52] V. Dhinakaran, K.P. Manoj Kumar, P.M. Bupathi Ram, M. Ravichandran, M. Vinayagamoorthy. A review on recent advancements in fused deposition modeling, *Materials Today: Proceedings*. 2020;27(2):752-756,
- [53] KS. Boparai, R. Singh, H. Signh. Development of rapid tooling using fused deposition modeling: a review. *Rapid Prototyping Journal*. 2016;22(2):281-299
- [54] CNC Kitchen (2020, may, 30)/ Helicolis, threaded insets and embedded nuts in 3D prints – strength & Strength assessment. Available: <https://www.cnckitchen.com/blog/helicoils-threaded-insets-and-embedded-nuts-in-3d-prints-strength-amp-strength-assessment>
- [55] CNC kitchen (2019, December 7). Threaded inserts for 3D prints – cheap vs expensive. Available: <https://www.cnckitchen.com/blog/threaded-inserts-for-3d-prints-cheap-vs-expensive>
- [56] MATLAB. (2010). *version 7.10.0 (R2017B)*. Natick, Massachusetts: The MathWorks

- [57] Inc.IBM Corp. (2017). IBM SPSS Statistics for Windows. Armonk, NY: IBM Corp. Retrieved from <https://hadoop.apache.org>
- [58] Fleury RBC, Shimano AC, Matos TD, Teixeira KO, Romero V, Defino HLA. The Role of Pedicle Screw Surface on Insertion Torque and Pullout Strength. *Rev Bras Ortop (Sao Paulo)*. 2020 Dec;55(6):695-701. doi: 10.1055/s-0040-1710072. Epub 2020 Jun 8. PMID: 33364646; PMCID: PMC7748926.
- [59] Karakaşlı A, Acar N, Hüsemoğlu RB. Biomechanical comparison of pullout strengths of six pedicle screws with different thread designs. *Jt Dis Relat Surg*. 2021;32(1):192-197. doi: 10.5606/ehc.2021.77004. PMID: 33463436.
- [60] International Organization for Standardization. (2019). *Plastics — Determination of flexural properties (ISO178)*.
- [61] Bandar Abdullah Aloyaydi BA, Sivasankaran S, Ammar HA. Influence of infill density on microstructure and flexural behavior of 3D printed PLA thermoplastic parts processed by fusion deposition modeling. *AIMS Materials Science* (2019). 6(1);1033-1048. doi: 10.3934/matserci.2019.6.1033/
- [62] S. Farah, D.G. Anderson, R. Langer, "Physical and mechanical properties of PLA, and their functions in widespread applications — A comprehensive review". *Advanced Drug Delivery Reviews*. (2016) 107,367-392, <https://doi.org/10.1016/j.addr.2016.06.012>
- [63] Murariu M, Dubois P. PLA composites: From production to properties. *Advanced Drug Delivery Reviews*. (2016). 107;17-46
- [64] [PRO webinar] how to 3D print in metal on the MakerBot METHOD. (2021, 26 februari). MakerBot. <https://www.makerbot.com/stories/engineering/everything-you-need-to-know-about-pla-3dprinting/#:%7E:text=Other%20notable%20advantages%20of%20PLA,performance%20over%20a%20long%20duration.>
- [65] Rodríguez, J.F., Thomas, J.P. and Renaud, J.E. (2001), "Mechanical behavior of acrylonitrile butadiene styrene (ABS) fused deposition materials. Experimental investigation", *Rapid Prototyping Journal*, Vol. 7 No. 3, pp. 148-158. <https://doi.org/10.1108/13552540110395547>
- [66] Itimaker Tough PLA. (z.d.). Ultimaker. Consulted on 10 maart 2021, van <https://ultimaker.com/nl/materials/tough-pla>
- [67] Pandzic et al (2019) published by DAAAM international "effect of Infill type and density on tensile properties of PLA material for FDM process
- [68] Dave HK et al. Effect of infill pattern and infill density at varying part orientation on tensile properties of fused deposition modeling-printed poly-lactic acid part. *Proceedings of the Institution of Mechanical Engineers. Journal of Mechanical Engineering Science*. June 2019. doi:10.1177/0954406219856383
- [69] Seol SH, Zhao P, Shin BC, Zhang SU. Infill pattern parameters for mechanical properties of 3D printed PLA parts. *Journal of the Korean Society of Manufacturing Process Engineers*. (2018) 17(4);9-16.
- [70] Cura (4.7). (2017). [Software]. Ultimaker.
- [71] ASTM International. D790-17 Standard Test Methods for Flexural Properties of Unreinforced and Reinforced Plastics and Electrical Insulating Materials. West Conshohocken, PA; ASTM International, 2017. doi: <https://doi.org/10.1520/D0790-17>
- [72] Gebisa AW, Lemu HG. Investigating Effects of Fused-Deposition Modeling (FDM) Processing Parameters on Flexural Properties of ULTEM 9085 using Designed Experiment. *Materials (Basel)*. 2018 Mar 27;11(4):500. doi: 10.3390/ma11040500. PMID: 29584674; PMCID: PMC5951346.

- [73] O-BASF. (2020, september). Test Report ATLaS - Analytical Testing Lab Service (ATLaS).
- [74] European committee for standardization, "Nen-en-iso 527," 2019.
- [75] CNC Kitchen (2020, January 10). Gradient infill for 3D prints. Available: <https://www.cnckitchen.com/blog/gradient-infill-for-3d-prints>
- [76] Lee CY, Liu CY. The influence of forced-air cooling on a 3D printed PLA part manufactured by fused filament fabrication, *additive manufacturing*. 2019; 25 pp:196-203
<https://doi.org/10.1016/j.addma.2018.11.012>.
- [77] CNC Kitchen (2019, october, 19). Helicolis, THE EFFECT OF EXTRUSION WIDTH ON STRENGTH AND QUALITY OF 3D PRINTS Available: <https://www.cnckitchen.com/blog/the-effect-of-extrusion-width-on-strength-and-quality-of-3d-prints>
- [78] Kuznetsov VE, Solonin AN, Urzhumtsev OD, Schilling R, Tavitov AG. Strength of PLA Components Fabricated with Fused Deposition Technology Using a Desktop 3D Printer as a Function of Geometrical Parameters of the Process. *Polymers*. 2018; 10(3):313.
<https://doi.org/10.3390/polym10030313>
- [79] CNC Kitchen (2019, september 28). THE INFLUENCE OF LAYER HEIGHT ON THE STRENGTH OF FDM 3D PRINTS. Available: <https://www.cnckitchen.com/blog/the-influence-of-layer-height-on-the-strength-of-fdm-3d-prints>
- [80] Van der stelt M, Wijnbergen DC, Verhamme L.. "The effect of annealing on deformation and mechanical strength of Tough PLA and its application in 3D printed prosthetic sockets" (2020). Unpublished.
- [81] CNC kitchen (2020, October 24). Testing the strength of 3D prints re-melted in salt. Available: <https://www.cnckitchen.com/blog/testing-the-strength-of-3d-prints-re-melted-in-salt>

Appendix A: First iteration design

First a 3D scan is made of the residual limb of the patient. The patients wore a stocking with an anatomical landmarks drew on it. This scan with texture is imported in Meshmixer (Autodesk). Then adjustments to the scan are made to create a proper fitting socket:

1. Positioning the 3D object in a 3D environment
2. In case of bony tibia end: make the socket 1 cm longer
3. Reduce volume by 5% (except pressure sensitive areas: Fibula head, Tibial crest and tip of fibula and tibia)
4. Increase or reduce volume on the marked areas:
 - a) Head of the fibular: No adjustments
 - b) Patella tendon: -7 mm
 - c) Medial tibial line: - (1.5-6) mm
 - d) Lateral tibial line: - (4-7) mm
 - e) Tibial crest: + (1-3) mm
 - f) Distal tip of tibia/fibula: + (2-3) mm
5. Smooth the 3D object
6. Cut out the shape of the socket
7. Give the prosthesis a 4mm thickness and connect the adapter
8. Final result

Then the socket is sliced using Cura (Ultimaker) and printed with the following settings:

Table A-1: print setting for the first iteration prosthetic socket

Printer	Ultimaker S5
Material	Ultimaker Tough PLA
Nozzle size	0.8 mm print core
Printing temperature	210 °C
Print speed	45 mm/sec
Bed temperature	60 °C
Layer thickness	0.2 mm
Infill percentage	100%
Infill pattern	concentric
Top, bottom and shell layers	6
Weight	352 +- 35
Material costs	20 USD
Printing costs	17 h +- 1.7 h

At last the prosthetic socket is connected by four M6 locknuts (Galvanised, DIN 985) and four M6 x 20 mm screws (Galvanised, DIN 7991) to the adapter.



Figure A-1: First iterations of the socket

Appendix B: Partial wall thickness

B.1 condyle caps

In this study the simplified socket with a 6 mm wall thickness was oriented in stance. Meaning the socket was aligned with the ground through zero displacement constraints at the bottom of the socket. All boundary conditions were set the same as the initial analysis of the socket in stance.

According to ten cate⁴¹ reinforcement of the popliteal depression has a negative effect of the stress distribution. In addition, thickening the lower half of the socket has a minor effect (0.5%) of stress reduction. By this means, those two areas are left out of the analysis.

Figure B-1 shows the division of the condyle caps. To determine the area of effectiveness, areas were extruded with 4 mm in variety of different combinations (see figure B-2). Subsequently, a new FEA has been run. The maximum stress values were examined and compared to the initial stress accumulation. A maximal stress reduction of 38.1% was found naturally in the reinforcement that covered the total surface of the condyle cap. To keep the material costs as low as possible, this is not the most suitable option.

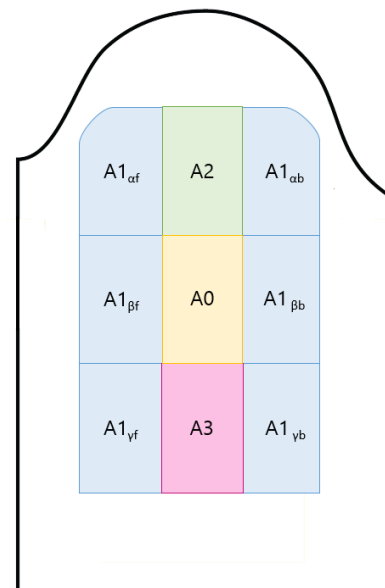


Figure B-1: Division of area components





Figure B-2: Results of 47 FEA reinforcement combinations to determine the area of effectiveness. Expressed in stress reduction in %.

B.2: patella

To investigate the influence of patellar reinforcement, the initial socket design was subjected to another FEA. The boundary conditions were set equal to the stance phase. At the height of patella a 4 mm thick reinforcement was designed all the way up to the condyle caps (see figure B-3). With every FEA the reinforcement was placed 2 cm downwards (B1, B1.5 and B2). Results of these analyses are shown in figure B-4. A small reduction of stress was found with the B1 and B1.5 reinforcement. The B2 reinforcement showed less reduction because the placement of the reinforcement is underneath the center of the initial stress accumulation.

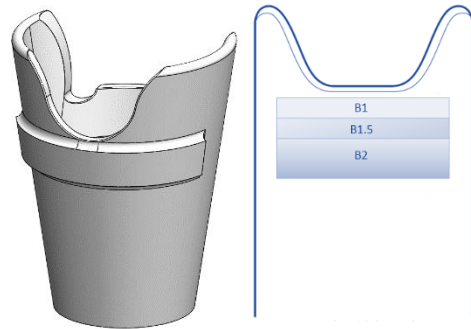
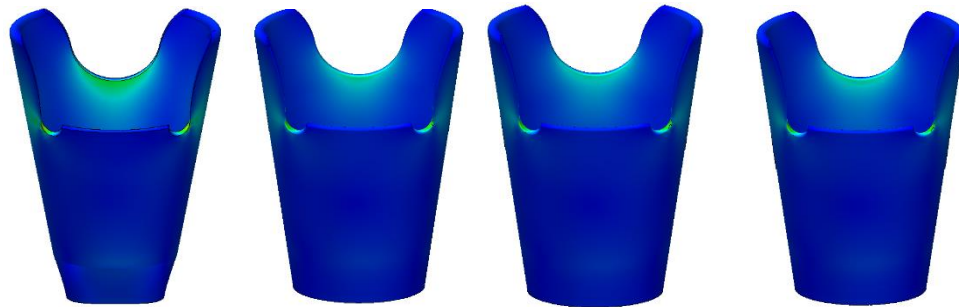


Figure B-3: STL example of patellar reinforcement and variation



Reinforcement	No	B1	B1.5	B2
Max stress	13.8 MPa	10.5 MPa	10.6 MPa	11.1 MPa

Figure B-4: Results of the FEA of the patellar reinforcement. When the reinforcement is placed at the centre of accumulation stress is further reduced than placed lower.

Appendix C: Results of bending tests

Appendix C provides all mean values of maximal flexural stress, flexural modulus and strain of the bending tests of chapter 4.

Table C-1: Mean flexural stress, modulus and strain of test 1 for each sample group with standard deviation.

	Max Flexural stress [MPa]		Flexural modulus [MPa]		Strain [%]	
	T	L	T	L	T	L
Con_{100%}	80.08 ± 0.67	86.60 ± 5.93	2292.68 ± 150.90	1997.35 ± 54.06	3.84 ± 2,46	4.90 ± 0,14
Lines_{60%}	54.17 ± 0.45	61.01 ± 1.25	1752.58 ± 139.18	1705.05 ± 66.64	3.82 ± 0,12	3.66 ± 0,20
Lines_{80%}	66.49 ± 0.82	67.90 ± 1.58	1914.17 ± 159.76	1737.93 ± 182.66	3.96 ± 0,29	4.01 ± 0,18
Grid_{60%}	54.45 ± 1.62	43.56 ± 0.85	1586.88 ± 127.03	1598.25 ± 149.64	3.61 ± 0,52	3.11 ± 0,36
Grid_{80%}	71.72 ± 0.30	66.53 ± 5.37	2075.82 ± 346.67	1672.55 ± 144.87	4.15 ± 0,29	3.47 ± 0,50
CS_{60%}	40.08 ± 1.69	56.64 ± 1.14	1506.10 ± 555.01	1644.07 ± 334.37	2.42 ± 0,06	4.21 ± 0,23
CS_{80%}	48.13 ± 2.16	64.49 ± 1.37	1887.07 ± 132.78	1411.28 ± 227.56	2.68 ± 0,28	4.23 ± 0,36

Table C-2: Mean flexural stress, modulus and strain of test 2 for each sample group with standard deviation.

	Max Flexural stress [MPa]		Flexural modulus [MPa]		Strain [%]	
	T	L	T	L	T	L
Lines_{50%}	72.63 ± 0.66	77.68 ± 1.56	2393.65 ± 115.85	2359.43 ± 76.97	4.03 ± 0.28	3.56 ± 0.09
Lines_{70%}	85.07 ± 2.24	90.56 ± 1.33	2707.40 ± 127.16	2432.97 ± 63.50	4.13 ± 0.44	4.54 ± 0.25
Lines_{90%}	77.96 ± 0.50	77.69 ± 1.89	2425.47 ± 124.94	2359.73 ± 205.22	4.30 ± 0.25	3.48 ± 0.01
Grid_{50%}	75.96 ± 1.96	73.83 ± 4.38	2551.43 ± 141.74	2458.33 ± 172.58	3.40 ± 0.33	3.10 ± 0.39
Grid_{70%}	84.96 ± 1.31	75.30 ± 0.44	2609.04 ± 303.86	2373.43 ± 242.08	4.65 ± 0.11	3.49 ± 0.06
Grid_{90%}	78.10 ± 14.2	77.96 ± 1.17	2719.07 ± 62.65	2431.28 ± 125.12	3.57 ± 1.32	3.65 ± 0.18

Table C-4: Mean flexural stress, modulus and strain of test 3 for each sample group with standard deviation.

	Max Flexural stress [MPa]				Flexural modulus [MPa]				Strain [%]			
	T		L		T		L		T		L	
30% 4 mm	82.91	± 0,84	93,88	± 1.23	2560.16	± 464.63	2900.08	± 312.32	4.07	± 0.08	4.24	± 0.09
30% 8 mm	59.95	± 1.77	63.20	± 1.06	1926.00	±129.09	2034.28	± 79.47	3.14	± 0.23	2.97	± 0.10
30% 10 mm	55.66	± 1.16	52.77	± 0.19	1767.35	± 139.96	1760.67	± 179.01	3.26	± 0.04	2.93	± 0.11
30% 12 mm	52.54	± 2.78	49.24	± 0.39	1435.15	± 178.97	1224.37	± 393.48	3.37	± 0.03	3.12	± 0.02
50% 4 mm	82.90	± 0.24	95.55	± 0.99	2795.40	± 184.96	2907.50	± 218.83	4.14	± 0.31	4.12	± 0.39
50% 8 mm	64.39	± 2.20	69.13	± 0.81	2246.08	± 184.73	2468.13	± 84.54	3.28	± 0.33	2.95	± 0.12
50% 10 mm	61.93	± 4.62	62.98	± 2.61	1682.30	± 304.64	1822.30	± 282.93	3.25	± 0.29	3.51	± 0.56
50% 12 mm	59.36	± 3.78	53.93	± 0.71	1572.70	± 200.86	1511.37	± 192.74	3.50	± 0.20	3.76	± 0.32
70% 4 mm	84.31	± 1.42	96.68	± 1.29	2966.93	± 20.13	3183.58	± 41.05	4.32	± 0.12	4.21	± 0.33
70% 8 mm	74.53	± 2.06	68.15	± 1.69	2168.92	± 110,83	2302.35	± 241.81	3.76	± 0.38	3.47	± 0.23
70% 10 mm	73.24	± 5.02	78.07	± 5.84	1868.53	± 23.13	1807.75	± 343.16	3.73	± 0.21	4.15	± 0.28
70% 12 mm	72.23	± 5.91	63.98	± 0.67	1789.57	± 124.13	1647.58	± 124.23	3.81	± 0.17	3.98	± 0.07
90% 4 mm	84.037	± 1.25	96.59	± 1.23	2773.52	± 214.57	2882.38	± 179.06	3.91	± 0.30	3.91	± 0.14
90% 8 mm	78.33	± 2.07	83.22	± 1.30	2295.08	± 275.43	2665.38	± 22.28	3.65	± 0.18	3.75	± 0.02
90% 10 mm	76,60	± 2.96	82.12	± 6.37	1748.62	± 501.54	2053.67	± 79.63	4.00	± 0.15	4.12	± 0.19
90% 12 mm	74.19	± 6.54	83.13	± 0.32	1821.43	± 98.63	1596.15	± 187.20	3.90	± 0.11	4.26	± 0.22

Table C-3: Mean flexural stress, modulus and strain of test 4 for PA11 and PA12 with standard deviation.

	Max Flexural stress [MPa]				Flexural modulus [MPa]				Strain [%]			
	T		L		T		L		T		L	
PA11	59.22	± 0.51	58.89	± 1.16	1407.07	± 11.23	1401.39	± 241.85	5.00	± 0.00	5.00	± 0.00
PA12	72.45	± 3.36	73.45	± 0.79	1793.15	± 65.56	1794.68	± 23.44	5.00	± 0.00	5.00	± 0.00